inorganics

MDPI

Article

TiO_2 Nanoparticles Obtained by Laser Sintering When Added to Methacrylate Photopolymer Resin Improve Its Physicochemical Characteristics and Impart Antibacterial Properties

Aleksandr V. Simakin [1,*], Dmitriy E. Burmistrov [1], Ilya V. Baimler [1], Ann V. Gritsaeva [1], Dmitriy A. Serov [1], Maxim E. Astashev [1,2], Pavel Chapala [3], Shamil Z. Validov [4], Fatikh M. Yanbaev [4] and Sergey V. Gudkov [1]

[1] Prokhorov General Physics Institute of the Russian Academy of Sciences, Vavilov Str. 38, 119991 Moscow, Russia; dmitriiburmistroff@gmail.com (D.E.B.); ilyabaymler@yandex.ru (I.V.B.); anngritsaeva@mail.ru (A.V.G.); dmitriy_serov_91@mail.ru (D.A.S.); astashev@yandex.ru (M.E.A.); s_makariy@rambler.ru (S.V.G.)
[2] Federal Research Center "Pushchino Scientific Center for Biological Research of the Russian Academy of Sciences", Institute of Cell Biophysics of the Russian Academy of Sciences, 3 Institutskaya Str., 142290 Pushchino, Russia
[3] HARZ Labs LLC, Silikatnaya Str. 51AC6, 141006 Mytischi, Russia; p.chapala@harzlabs.com
[4] Federal Research Center Kazan Scientific Center of the Russian Academy of Sciences, ul. Lobachevskogo 2/31, Tatarstan, 420088 Kazan, Russia; sh.validov@knc.ru (S.Z.V.); f.yanbayev@knc.ru (F.M.Y.)
* Correspondence: avsimakin@gmail.com

Abstract

In this paper, titanium oxide nanoparticles (TiO_2-NPs) with complex surface topologies were obtained for the first time using simple procedures applied in laser sintering. Based on the obtained nanoparticles and polymethyl methacrylate-like photopolymer resin, a composite material (MPR/TiO_2-NPs) for 3D printing was created using the MSLA technology. Products made of the material containing from 0.001 to 0.1% wt. TiO_2-NPs didn't contain internal defects and were less brittle than the resin without nanoparticles. Products made of the MPR/TiO_2-NPs material were well polished; after polishing, areas with a variation in the surface profile height of less than 10 nm were found on the surfaces. Nanoparticles in the volume of products made of the material are apparently unevenly distributed; there are alternating areas of micrometer sizes with slightly higher and slightly lower concentrations of nanoparticles. Spectroscopy showed that adding the developed nanoparticles promoted better polymerization of the MPR resin. The addition of nanoparticles to the material slightly increased its ability to generate active forms of oxygen and damage biomacromolecules. At the same time, the resulting material exhibits significant antibacterial properties and doen't affect the growth and reproduction of animal cells. The created material can be a very effective basis for the additive manufacturing of products with improved physical and chemical properties and balanced biological activity.

Keywords: TiO_2; nanoparticles; composite photopolymer resin; laser sintering; antibacterial materials

check for updates

Academic Editors: Eduardo Padilla-Camberos and Angélica Sofía González-Garibay

Received: 9 June 2025
Revised: 2 July 2025
Accepted: 8 July 2025
Published: 10 July 2025

Citation: Simakin, A.V.; Burmistrov, D.E.; Baimler, I.V.; Gritsaeva, A.V.; Serov, D.A.; Astashev, M.E.; Chapala, P.; Validov, S.Z.; Yanbaev, F.M.; Gudkov, S.V. TiO_2 Nanoparticles Obtained by Laser Sintering When Added to Methacrylate Photopolymer Resin Improve Its Physicochemical Characteristics and Impart Antibacterial Properties. *Inorganics* **2025**, *13*, 233. https://doi.org/10.3390/inorganics13070233

Copyright: © 2025 by the authors. Licensee MDPI, Basel, Switzerland. This article is an open access article distributed under the terms and conditions of the Creative Commons Attribution (CC BY) license (https://creativecommons.org/licenses/by/4.0/).

1. Introduction

In view of the rapidly developing 3D additive manufacturing industry, there is a growing demand for new functional materials with improved strength characteristics and controlled biological activity. Polymethyl methacrylate-like photocurable resins have become widespread in recent years [1–3]. Products made from such materials are approved

for use in various modern medical fields, including dentistry [4], orthodontics [5], orthopedics [6], and audiology [7]. To improve the physicochemical characteristics of methacrylate polymer materials, in particular, their reinforcement, the introduction of titanium dioxide nanoparticles (TiO_2-NPs) is often proposed [8–11]. The addition of TiO_2 allows for significant modification of the properties of polymers, expanding their functionality and service life, which makes these composites in demand in high-tech industries [12,13]. One of the most sought-after properties of polymer products obtained using 3D photopolymer printing is the resistance of their surfaces to bacterial cell adhesion and bacterial colony growth [14,15]. TiO_2-NPs are known to exhibit significant antibacterial activity against Gram-positive and Gram-negative bacteria, as well as a number of fungal pathogens [16]. Therefore, they have attracted considerable interest for a variety of practical purposes due to their unique properties and universal applications [17–19]. The pronounced antibacterial properties of these nanoparticles allow them to be used as effective agents in various medical applications, including wound healing [20], drug delivery [21], and visualization [22]. Numerous modern studies have demonstrated the use of TiO_2-NPs as functional additives in polymer matrices to create antibacterial composite materials for packaging and dressings [23,24]. Despite the high efficiency of TiO_2-NPs as functional additives in polymers, their mass use raises concerns regarding their possible negative impact on the environment and the presence of possible toxicity toward animal cells [25]. Therefore, a detailed study of composite materials on the growth and development of cell cultures in vitro is required.

The weak chemical affinity between nanoparticles and chains of methacrylate-based photopolymers often leads to incomplete curing of the interphase layer during photopolymer 3D printing, which negatively affects both the stability of the system and the mechanical properties of the finished product [26]. One solution to this problem is to use nanoparticles with a size comparable to that of the polymer chains [27]. In this case, due to the weak fixation of nanoparticles inside the polymer, desorption or leaching of nanoparticles from the polymer can be observed [28]. Another solution is to use nanoparticles with complex surface topologies [29]. With this solution, the contact area between the nanoparticles and polymer chains significantly increased. The problem of obtaining nanoparticles from one material with a complex surface topology using laser ablation, fragmentation, or sintering has not been solved to a significant extent [30]. Only a few examples of nanoparticles with complex topologies have been obtained, and the technology for obtaining them is difficult to repeat and doesn't allow the production of significant quantities of nanoparticles [27,31,32]. In this study, titanium oxide nanoparticles with complex surface topologies were obtained for the first time using laser sintering and simple experimental procedures. An antibacterial composite material for 3D printing was created using MSLA technology based on the obtained nanoparticles and polymethyl methacrylate-like photopolymer resin. Such materials can serve as a very effective basis for the additive manufacturing of products with improved physicochemical properties and balanced biological activity.

2. Results

The morphology of titanium oxide nanoparticles obtained by laser ablation of a massive titanium target in water was studied using TEM. The titanium oxide nanoparticles obtained by laser ablation have a shape close to spherical with an average size of about 20 nm (Figure 1a). The size distribution of the nanoparticles in the entire colloid was studied. Using the dynamic light scattering method, it was shown that the distribution of nanoparticles in the colloid has a monomodal particle distribution with a maximum of about 20 nm and a half-width of the distribution of about 10 nm (Figure 1b). After the nanoparticles in the colloid were subjected to laser sintering, the size of the nanoparticles was analyzed again. The analysis of the TEM images of the nanoparticles obtained as a

result of laser sintering shows that the obtained particles have a close to spherical shape with an average size of about 200 nm (Figure 1c). On the surface of the nanoparticles, smaller nanoparticles were observed to be fused, and the surface of the nanoparticles did not appear smooth. The size distribution of TiO_2-NPs was monomodal, with a maximum of about 150 nm (Figure 1d). The optical properties of the nanoparticle colloid were also studied. The colloid was shown to weakly absorb in the wavelength range of 350–800 nm (Figure 2a). Radiation with a wavelength of less than 350 nm is absorbed much more intensely. The distribution of the electrokinetic potential in the TiO_2-NPs colloid was also studied. The distribution of the electrokinetic potential was monomodal with one pronounced maximum of about −30 mV (Figure 2b), which indicates the high stability of the obtained colloidal solution of nanoparticles.

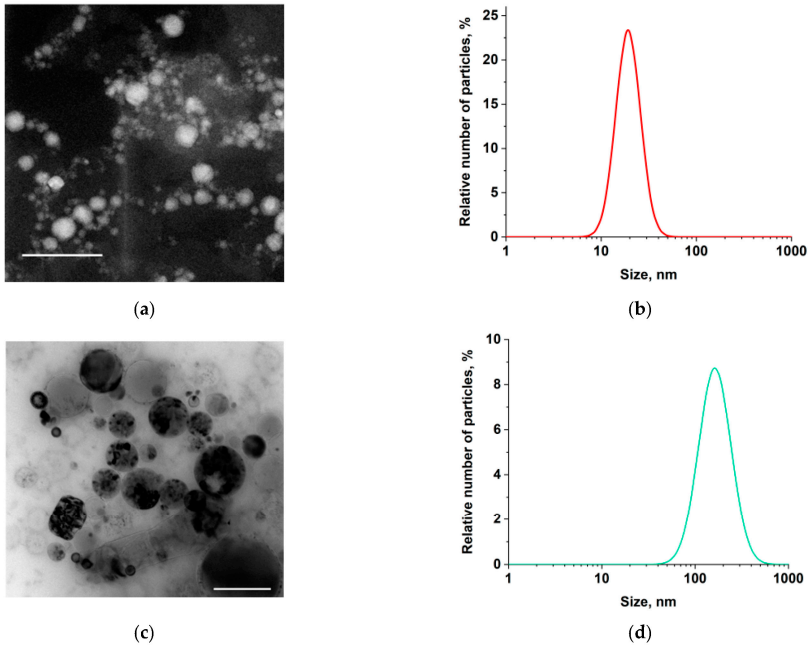

Figure 1. Characteristics of TiO_2-NPs obtained via laser ablation and laser sintering. (**a**) TEM image of TiO_2 nanoparticles obtained by laser ablation of titanium in water (scale bar = 100 nm); (**b**) size distribution of TiO_2 nanoparticles obtained by laser ablation; (**c**) TEM image of TiO_2-NPs obtained by laser sintering (scale bar = 300 nm); (**d**) size distribution of TiO_2 nanoparticles obtained by laser sintering.

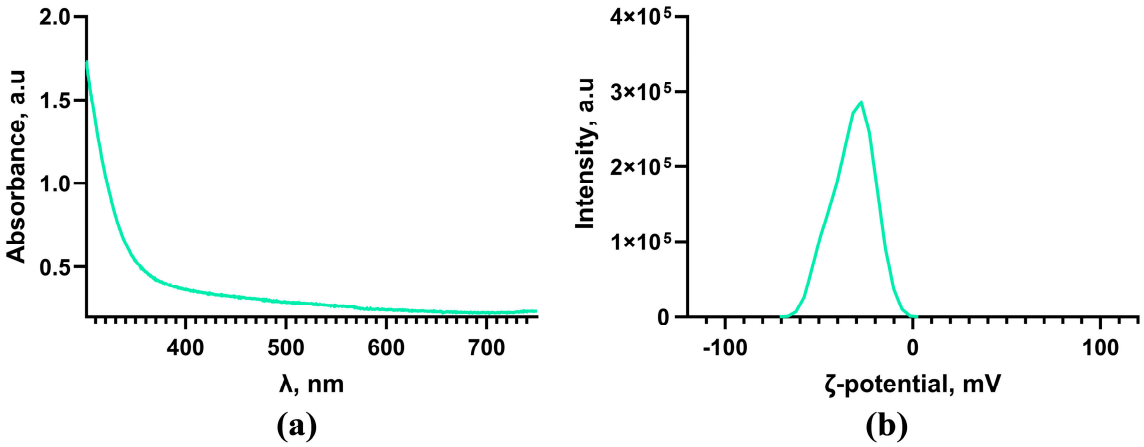

Figure 2. UV-Vis absorption spectra of TiO_2-NPs aqueous colloid obtained by laser sintering (**a**) and ζ-potential distribution of TiO_2-NPs obtained by laser sintering (**b**).

TiO_2-NPs were introduced into the methacrylate photopolymer resin (MPR) at three different concentrations: 0.001, 0.01, and 0.1 wt%. To comprehensively study the mechanical properties of the obtained MPR/TiO_2-NPs composite material, standard-sized samples were fabricated by MSLA 3D printing: rectangular bars of 80 × 10 × 4 mm and dumbbell-shaped samples of 80 × 5 × 3 mm, corresponding to the international standards ISO 179-1:2010 [33] Type 1 and ISO 527-2:2012 [34] Type 1A, respectively (Figure 3a). In parallel, round plates with a diameter of 16 mm were printed for the biological studies. To demonstrate the material's capabilities, a porous sample of 8 × 8 × 4 mm with a regular structure was successfully reproduced (Figure 3b). The pitch of the regular structure was 80 µm, and the edge of the structure had a thickness of about 15 µm, which corresponds to the maximum detail of the photo printer used. Thus, the photopolymer resin with TiO_2-NPs in the polymer matrix—0.001–0.1 wt.% allows printing products with micrometer accuracy. The printed samples retained the specified geometry and integrity of the structure.

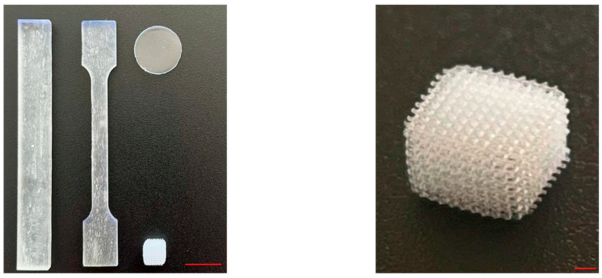

(**a**) (**b**)

Figure 3. Photographs of printed MPR/TiO_2-NPs composite specimens: (**a**) ISO 179-1:2010 Type 1 point-bend specimen (left) and ISO 527-2:2012 Type 1A tensile specimen (center), ∅16 mm biological wafer specimen (top right), and mesh-structure specimen (bottom right). The scale bar in the lower right corner of the photographs corresponds to 10 mm. (**b**) Enlarged image of a mesh-structured specimen printed from MPR/TiO_2-NPs containing 0.1 wt.% TiO_2-NPs. The scale bar in the lower right corner of the photographs corresponds to 1 mm.

When mechanical tests were conducted in accordance with the standard ASTM D790 [35] and ASTM D638-22 [36] protocols, it was found that the composite materials containing 0.1 wt.% TiO_2-NPs demonstrate a significantly different deformation pattern compared to the pure polymer material. In particular, samples with the addition of 0.1 wt.% TiO_2-NPs exhibited pronounced inhomogeneous plastic deformation, while the control samples (without nanoparticles) failed by brittle rupture (Figure 4a,b).

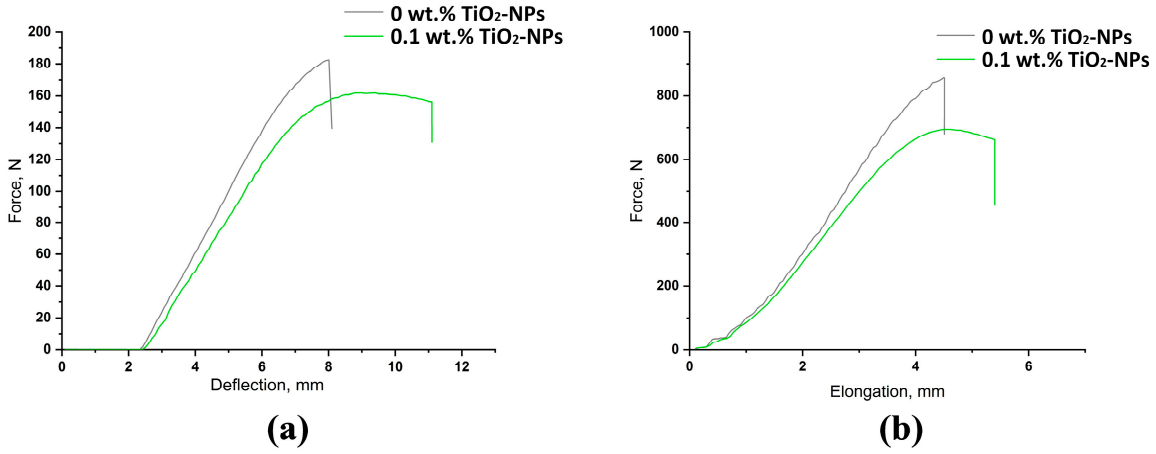

Figure 4. Stress-strain curves for composite material samples printed using MPR/TiO_2-NPs containing 0.1 wt.% TiO_2-NPs and a control polymer sample, obtained in bending (**a**) and tensile (**b**) tests.

At the same time, quantitative characteristics reflecting the mechanical properties of the composite materials with the addition of 0.1 wt.% TiO_2-NPs also significantly changed. In both bending and tensile tests, a decrease in yield strength of ~15% was observed for the composite materials compared with the control samples. At the same time, the tensile and tear strengths increased in the case of the composite materials. The Young's modulus values were about 2200 MPa and 2500 MPa for the composite material containing 0.1 wt.% TiO_2-NPs and the control polymer sample, respectively. The results indicate that the introduction of nanoparticles at a concentration of 0.1 wt.% affects the nature of the deformation behavior of the polymer matrix of the material and leads to a decrease in the brittleness of the material.

To study the characteristics of the composite materials, an additional 0.5 mm-thick round plates were produced using the same printing parameters. The samples were polished carefully. Topographic analysis of the surfaces of the obtained samples was performed using atomic force microscopy (AFM), which revealed a high degree of surface homogeneity without significant structural defects (Figure 5a,b). The obtained data demonstrate that the introduction of TiO_2-NPs into the polymer doesn't affect the affinity of the material for polishing. On the surfaces of both MPR and MPR/TiO_2-NPs, areas with a variation in the height of the surface profile of less than 10 nm per 1 μm2 were observed.

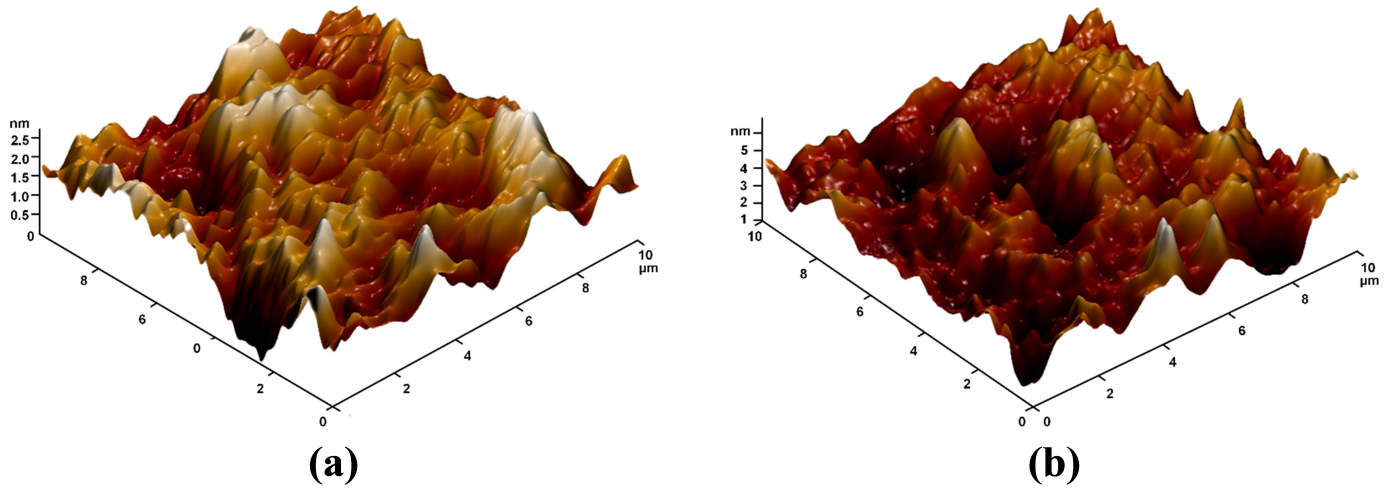

Figure 5. Reconstructions of the surfaces of printed material plate samples obtained using atomic force microscopy: surface of the polymer from MPR without the addition of TiO_2-NPs (control) (**a**); surface of the composite material printed from MPR/TiO_2-NPs containing 0.1 wt % TiO_2-NPs (**b**).

The distribution of TiO_2-NPs in the polymer matrices of the composite materials printed from MPR/TiO_2-NPs was studied by modulation interference microscopy (MIM), which allows the visualization of optical inhomogeneities due to a significant difference in the refractive indices of the pure polymer (n = 1.49) and TiO_2 (n = 2.8). Analysis of the micrographs revealed fundamental differences between the control and modified samples. The pure polymer material demonstrated an optical structure without visible inhomogeneities (Figure 6a), which indicates the absence of voids, bubbles, and other structural imperfections in the bulk of the material. The introduction of TiO_2-NPs led to pronounced optical inhomogeneities, the size and number of which correlated with the filler concentration. In composites with 0.001% TiO_2-NPs, small inhomogeneities of about 0.5 × 0.2 μm in size were observed (Figure 6b). An increase in concentration to 0.01% was accompanied by an increase in inhomogeneities to 2.0 × 1.0 μm (Figure 6c). The greatest structural changes were recorded for the sample with 0.1% TiO_2-NPs, where extended areas of optical inhomogeneities with a width of 1–2 μm and a length of over 8 μm were

observed (Figure 6d). Thus, it was shown that all the manufactured materials did not contain defects in the form of voids and cracks in their structure. The nanoparticles were unevenly distributed in the volume, with alternating areas of slightly higher and lower concentrations of nanoparticles present.

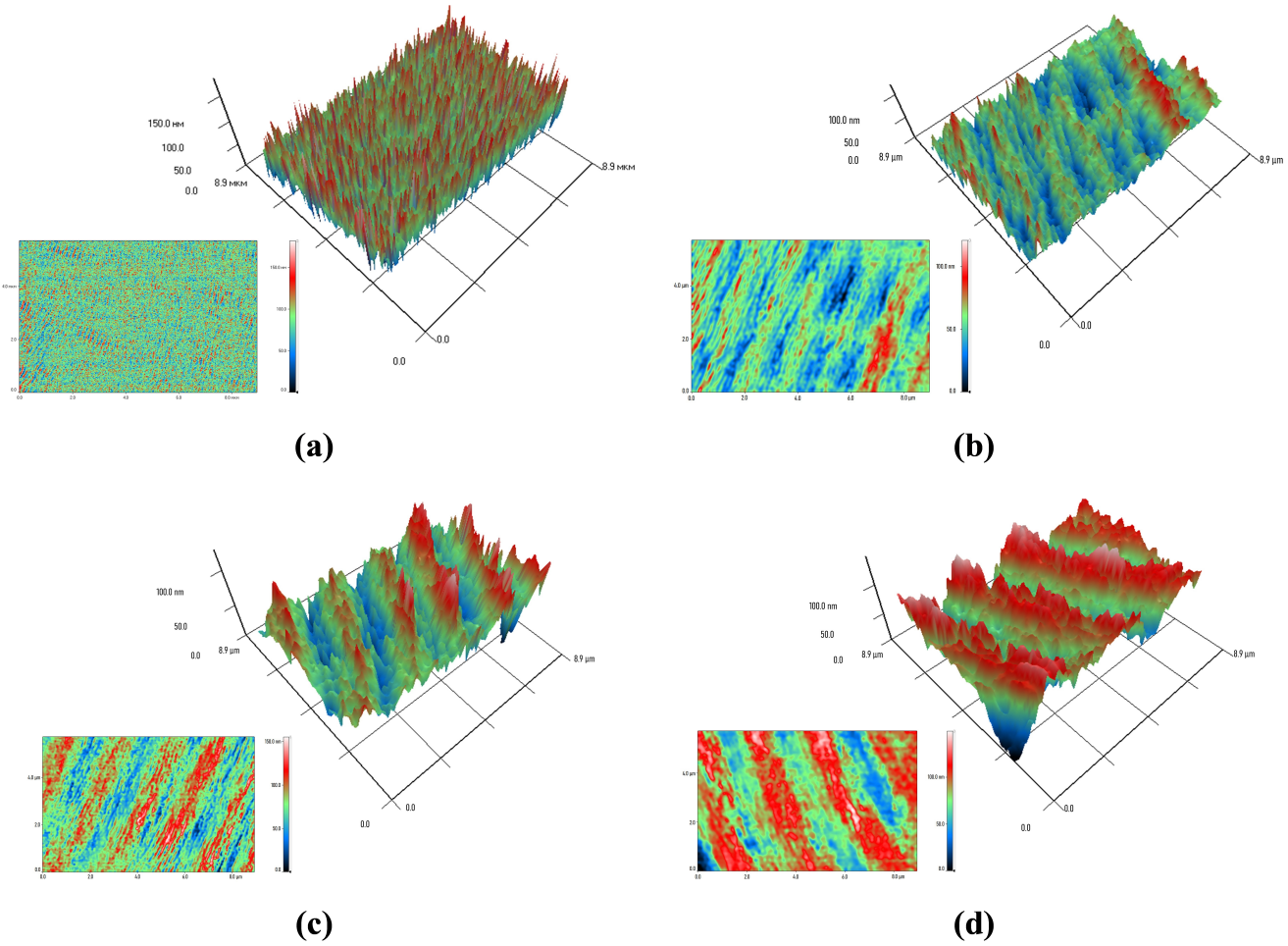

Figure 6. MIM micrographs and 3D reconstructions of composite material samples printed from MPR/TiO_2-NPs: Polymer sample obtained from MPR without the addition of NPs (**a**), composite polymer materials printed from MPR with the addition of TiO_2-NPs at concentrations of 0.001 wt. % (**b**), 0.01 wt.% (**c**) and 0.1 wt.% (**d**). 3D reconstructions of material sections measuring 8.9 × 8.9 µm and the primary data on which they are based are shown (insets at the bottom left). The color indicates the phase difference of the transmitted radiation in nm (red—maximum phase difference of 200 nm, blue—no phase difference).

To study the effect of TiO_2-NPs on the molecular structure of the methacrylate polymer matrix, a comprehensive spectral analysis was performed in the infrared, visible, and ultraviolet regions. Figure 6a shows the averaged FTIR transmission spectra for a series of studied composite materials. Particular attention was paid to the characteristic peaks at 1611 and 1637 cm^{-1}, corresponding to the stretching vibrations of the C=C double bonds (Figure 7a, inset). The analysis revealed a significant decrease in the intensity of the characteristic C=C bands in all composites containing TiO_2-NPs compared to the control sample of pure polymer. The most pronounced effect was observed for the composite with 0.1% nanoparticles, where the decrease in intensity reached ~70%. These data indicate a significant effect of TiO_2-NPs on the kinetics and depth of the polymerization processes in the methacrylate matrix.

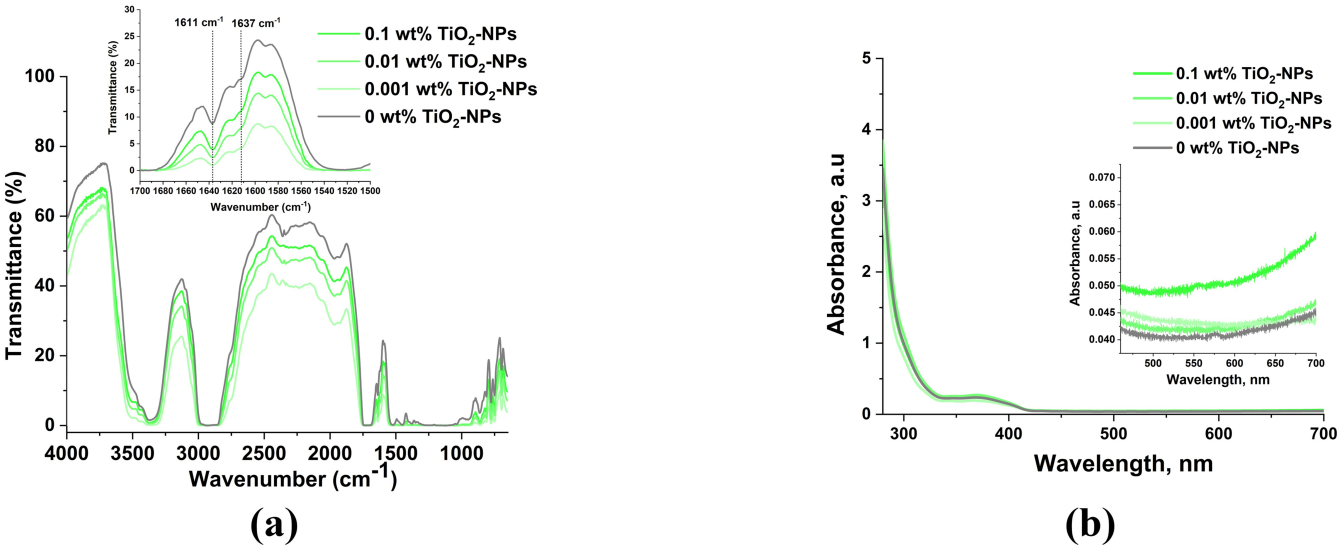

Figure 7. Results of spectroscopic study of samples printed from MPR with different concentrations of TiO_2-NPs. (**a**) FTIR transmission spectra of the samples of composite material plates printed from MPR/TiO_2-NPs with different TiO_2-NPs content. The inset at the top is an enlarged region of the spectrum with lines related to C=C double bonds. (**b**) UV/Vis absorption spectra of composite material samples with different TiO_2-NPs content, the inset on the right is an enlarged part of the spectrum in the visible region of 450–700 nm.

Figure 7b shows the UV-Vis absorption spectra of the obtained composite materials. Analysis of the spectral characteristics showed that the introduction of TiO_2-NPs in the studied concentration range (0.001–0.1 wt.%) doesn't lead to a significant change in the optical properties of the methacrylate matrix in the visible region of the spectrum. All samples retained high transparency in the 450–700 nm range, indicating good compatibility of the composite components. Characteristic absorption bands were observed in the UV region of the spectrum (350–400 nm), corresponding to the photoinitiators present in the initial MPR, which ensured the photopolymerization process.

The effect of the obtained materials on the generation of active oxygen species, such as hydrogen peroxide and hydroxyl radicals, in aqueous solutions was studied (Figure 8). The experimental data demonstrated a significant increase in the generation of these active oxygen species when using composite materials compared to the control samples. It is interesting to note that the polymer without the addition of TiO_2-NPs exhibited the ability to generate ROS, which exceeded the baseline level by 30%. The introduction of TiO_2-NPs led to a pronounced increase in pro-oxidant activity, depending on the concentration of nanoparticles. When quantifying the formed hydrogen peroxide (Figure 8a), the following values were observed: 6.1 ± 0.6 nM for the composite with 0.001% TiO_2-NPs, 12.5 ± 0.8 nM at 0.01%, and 17.1 ± 0.9 nM for the material with 0.1% TiO_2-NPs. A similar effect was observed for hydroxyl radicals (Figure 8b): 29.6 ± 2.5 nM, 43.8 ± 4.2 nM, and 61.0 ± 5.2 nM, respectively. The greatest effect was observed at the maximum concentration of nanoparticles (0.1%), where the generation of H_2O_2 increased by ~3.5 times and $^{\bullet}OH$ by ~2.2 times compared to the polymer without nanoparticles.

The effect of composite materials obtained from MPR/TiO_2-NPs on the oxidative modification of DNA and proteins was studied (Figure 9). Using ELISA with antibodies to 8-oxoguanine, it was found that the polymer without nanoparticles did not lead to a significant increase in the level of detectable oxidative damage in the DNA. The polymer without nanoparticles and the polymer containing the minimum studied concentration of TiO_2-NPs affected the generation of 8-oxoguanine in DNA similarly. Samples with TiO_2-NPs contents of 0.01 and 0.1 wt.% caused a reliable increase in the formation of

8-oxoguanine, both relative to the control samples and relative to the samples containing the polymer without nanoparticles.

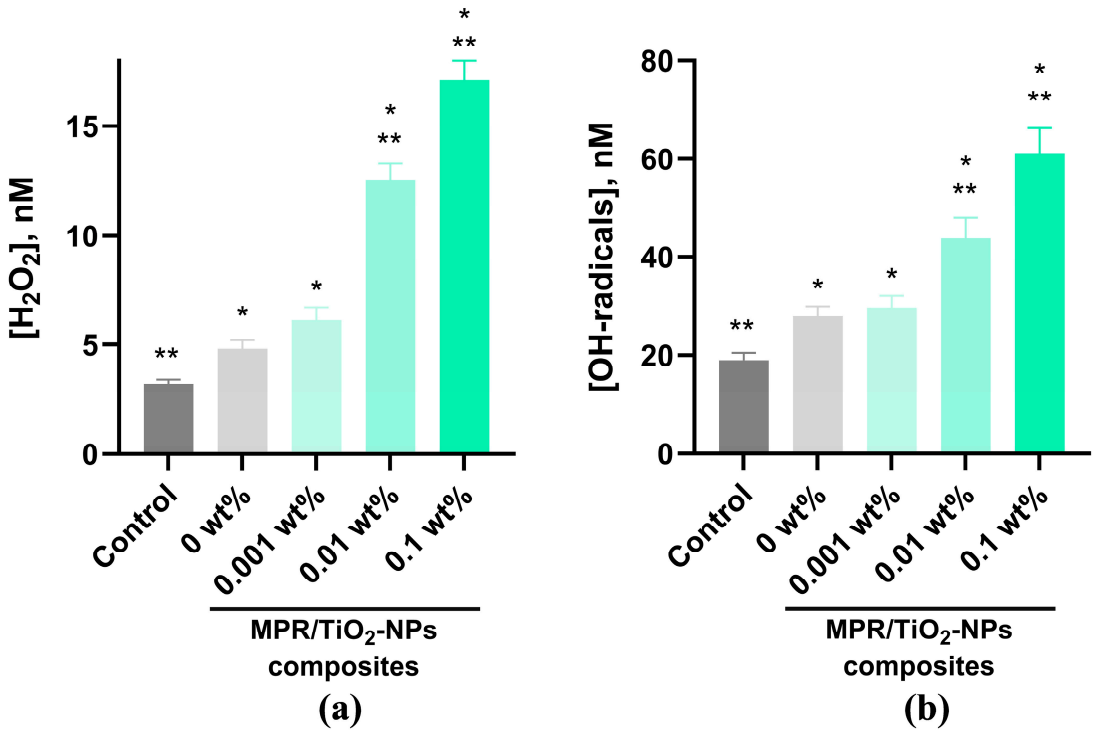

Figure 8. Results of the quantitative assessment of the concentration of hydrogen peroxide (**a**) and hydroxyl radicals (**b**) formed in aqueous solutions after incubation with samples of composite material plates printed from MPR/TiO_2-NPs with different TiO_2-NPs contents. Data are presented as mean values ± SEM (n = 3). *—difference from Control, $p < 0.05$; **—differences relative to polymer samples not containing TiO_2-NPs (0 wt.%), $p < 0.05$.

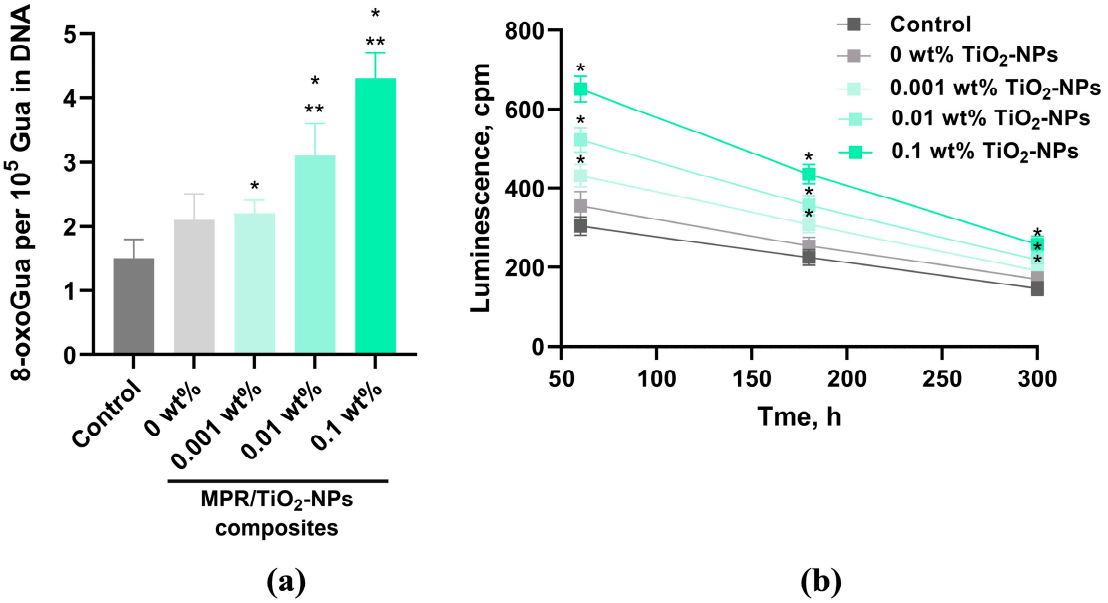

Figure 9. Results of assessing the effect of the obtained composite materials on biomolecules in vitro. Effect of MPR/TiO_2-NPs on the concentration of 8-oxoguanine in DNA (**a**) and the level of long-lived reactive forms of proteins (**b**). Data are presented as mean values ± SEM (n = 3). *—difference from the Control, $p < 0.05$; **—differences relative to polymer samples not containing TiO_2-NPs (0 wt.%), $p < 0.05$.

The effect of the obtained composite materials on the level of oxidative modification of bovine serum albumin, namely, on the formation of long-lived reactive protein forms (LRPS), was studied (Figure 9b). The observed effect was dose-dependent and correlated with the concentration of nanoparticles in the polymer matrix. Under control conditions without the polymer, LRPS formation with a half-life of approximately 5 h was observed. The amount of LRPS generated in the control and samples without TiO_2-NPs did not differ statistically. Polymer samples without TiO_2-NPs also induced the formation of LRPS with a half-life of about 5 h. When using composite materials printed from MPR/TiO_2-NPs with a TiO_2-NPs content of 0.001 to 0.1 wt.%, an increase in LRPS generation was observed. The half-life of such LRPS was also 5 h. It should be noted that the level of LRPS formed under control conditions and during incubation with MPR/TiO_2-NPs at 0.1 wt.% differed by more than 2 times. The obtained data are consistent with the results of the quantitative assessment of ROS and indicate the possible pro-oxidant properties of the obtained composite materials.

The results of the microbiological studies demonstrated a pronounced effect of the composite materials on the kinetics of *E. coli* growth (Figure 10). Analysis of bacterial culture growth curves during a 24-hour incubation period showed that the methacrylate polymer without nanoparticles did not have a statistically significant effect on the duration of the lag phase but caused a decrease in the maximum density of the bacterial culture by 27% compared to the control. The introduction of 0.001–0.1% TiO_2-NPs into the polymer matrix led to a reliable decrease in the maximum density of bacterial growth by 80–90% compared to that of the control, which indicates a pronounced bacteriostatic effect. At the same time, the time parameters of the lag phase of bacterial culture growth also changed for all composite materials; the difference in the duration of the lag phase between the groups with MPR/TiO_2-NPs and the control group was 5 h.

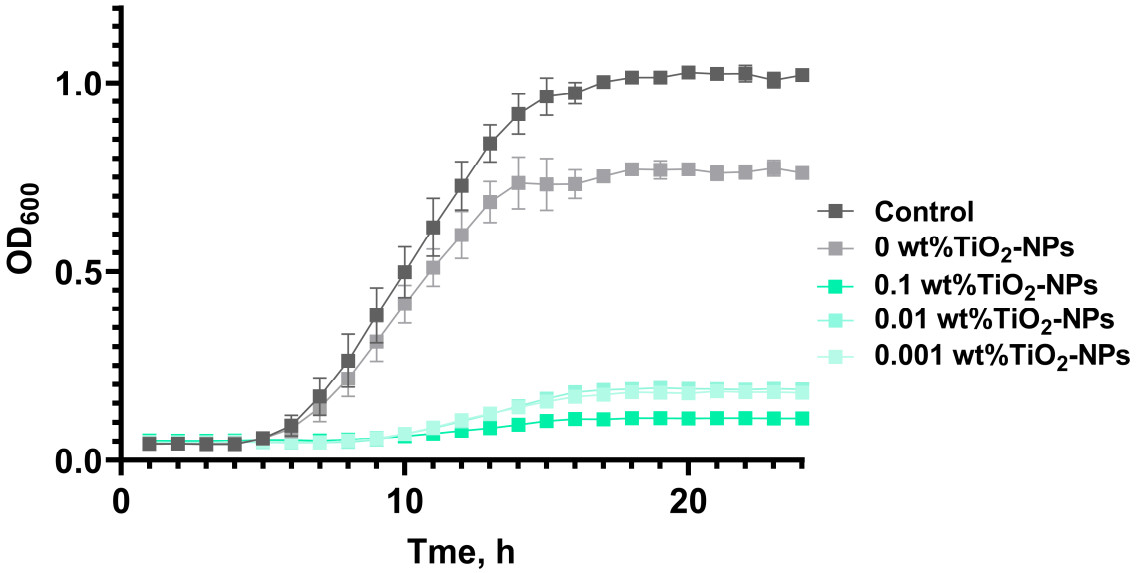

Figure 10. Growth curves of *E. coli* suspension cultures grown in the presence of composite material plate samples printed from MPR/TiO_2-NPs with different nanoparticle contents. Data are presented as mean ± SEM (n = 3).

To quantify the bactericidal activity of the composite materials, flow cytometry was performed using propidium iodide (PI), which allows differentiation between viable and non-viable *E. coli* cells. The analysis was performed after 24 hours of incubation of bacterial cultures with the samples under study. The results demonstrated a dose-dependent increase in the proportion of PI-positive (non-viable) cells when composites containing TiO_2-NPs

were used compared to the control samples of pure polymer. The greatest bactericidal effect was observed for the composite material with 0.1% TiO_2-NPs, where the proportion of dead cells reached ~97.2%, indicating a pronounced antimicrobial effect (Figure 11).

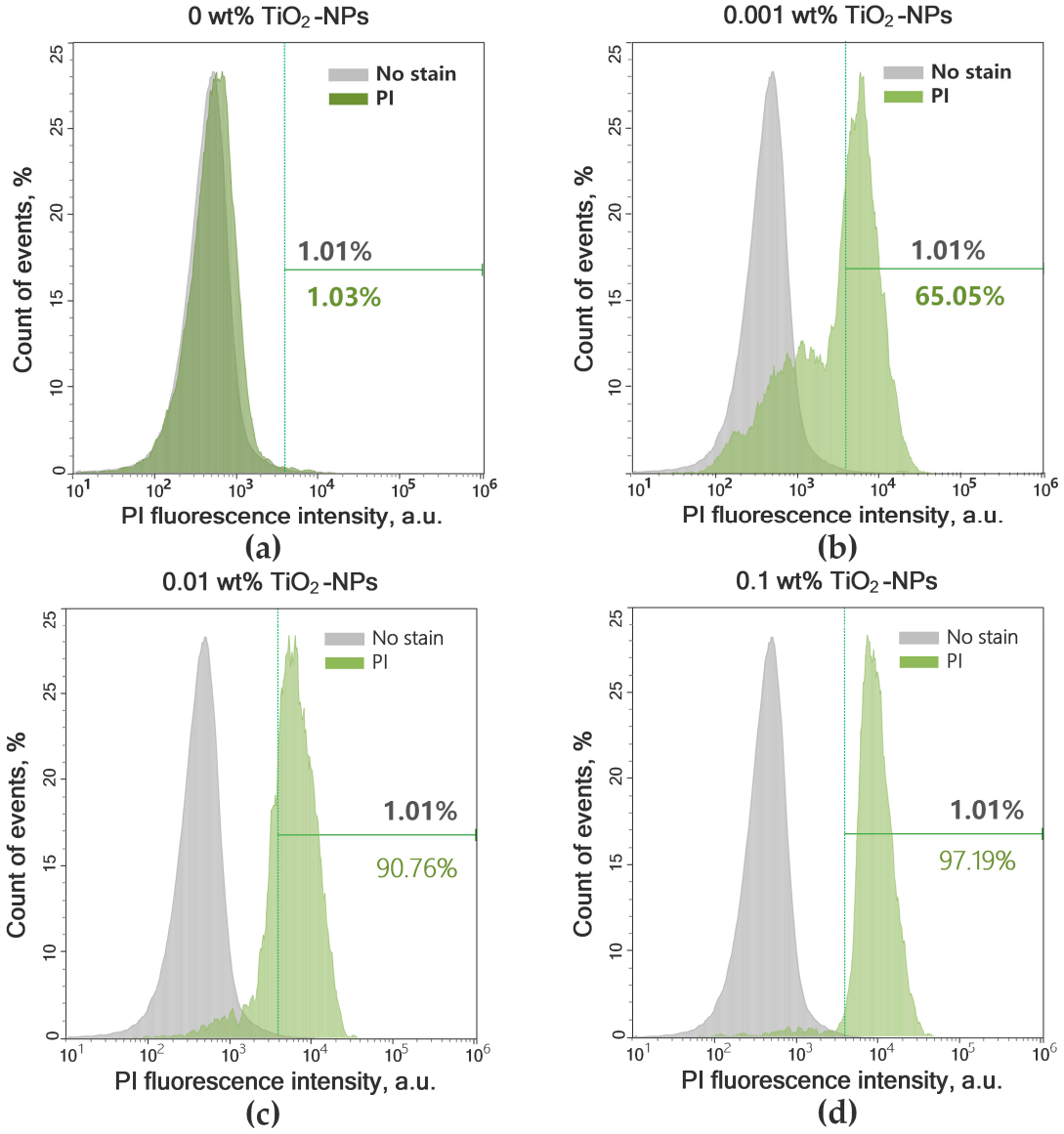

Figure 11. Effect of composite materials printed from MPR/TiO_2-NPs with different nanoparticle contents on the number of dead (PI-positive) *E. coli* cells. Histograms of bacterial cell distribution by the geometric mean PI intensity during incubation with polymer samples not containing TiO_2-NPs (**a**), and during incubation with composite material samples containing 0.001 (**b**), 0.01 (**c**), and 0.1 wt.% (**d**) TiO_2-NPs, respectively.

When incubating the bacterial suspension with samples of polymer material not containing TiO_2-NPs, a statistically significant decrease in the concentration of bacterial cells by two times (to 2.9×10^7 cells/mL) was observed, compared to the control group (5.8×10^7 cells/mL) (Figure 12a). The introduction of TiO_2-NPs into the polymer methacrylate matrix led to a pronounced, dose-dependent increase in the antimicrobial activity of the material. Cytometric analysis demonstrated a significant decrease in the concentration of *E. coli* when incubated with samples of the composite materials. The sample with 0.001% TiO_2-NPs reduced the bacterial concentration to 3.7×10^6 cells/mL, while the composite samples containing 0.01% and 0.1% TiO_2-NPs caused a decrease of two orders of magnitude (to 4.5×10^5 and 2.7×10^5 cells/mL), respectively, compared to the control. Notably, in

addition to the bacteriostatic effect, the materials exhibited a pronounced bactericidal effect. After 24-hour incubation, significant death of bacterial cells was observed: 62.0 ± 6.2% for 0.001% TiO_2-NPs, 95.7 ± 1.8% for 0.01% TiO_2-NPs, and 98.5 ± 1.0% for 0.1% TiO_2-NPs (Figure 12b). These data provide convincing evidence that the antimicrobial activity of the composites is due not only to growth inhibition but also to a direct damaging effect on the bacterial cells.

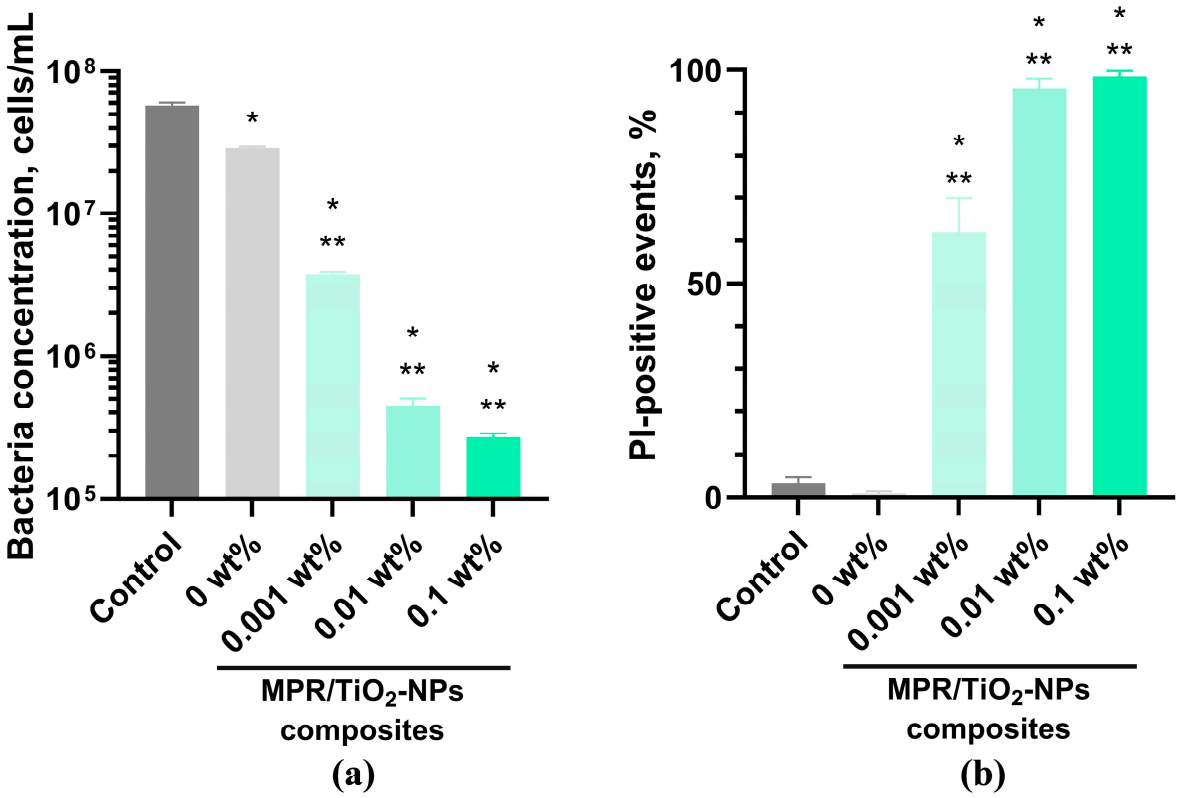

Figure 12. Flow cytometry results reflecting the antibacterial activity of composite materials printed from MPR/TiO_2-NPs with different TiO_2-NPs content: concentration of bacterial cells in suspension contacting the surfaces of samples of the studied materials (**a**) and the number (proportion) of PI-positive (non-viable) bacterial cells *E. coli* cultured in the presence of samples of plates of the studied materials (**b**). Data are presented as mean values ± SEM (n = 3). *—difference from the Control, $p < 0.05$; **—differences relative to polymer samples not containing TiO_2-NPs (0 wt.%), $p < 0.05$.

The effect of the obtained MPR/TiO_2-NPs on the viability of human spleen fibroblast (HSF) cultures was studied (Figure 13). No significant toxic effects were observed for any of the studied materials. Microscopic analysis did not reveal any changes in cell morphology during long-term cultivation in the presence of the studied samples compared to the control (Figure 13a,b). Quantitative assessment of cell viability demonstrated the preservation of a high proportion of viable cells in all experimental groups: 97.0 ± 2.2% for the composite material containing 0.001% TiO_2-NPs, 94.3 ± 2.7% for 0.01% TiO_2-NPs, and 92.0 ± 2.7% for 0.1% TiO_2-NPs, which did not statistically differ from the control values (96.2 ± 2.2%) (Figure 13c).

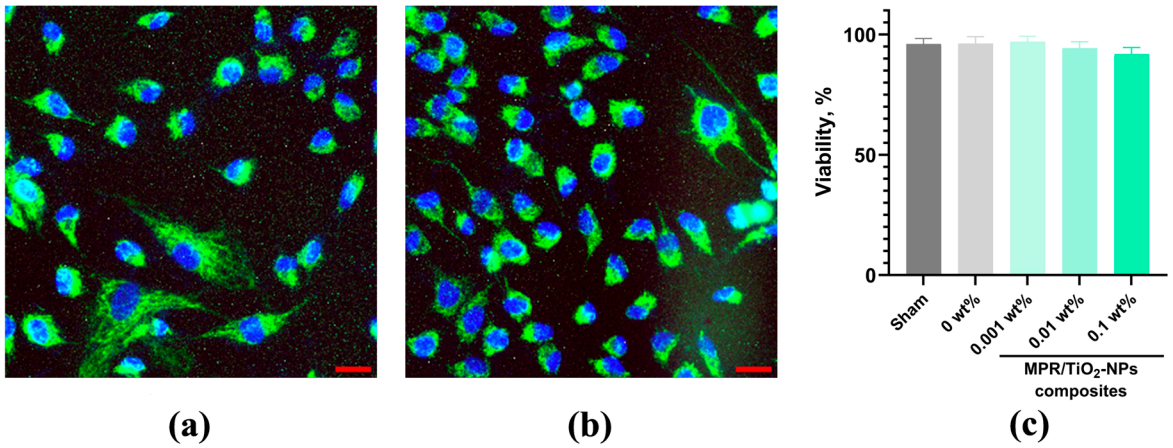

Figure 13. Results of viability assessment of HSF cell cultures in contact with samples of composite materials printed from MPR/TiO_2-NPs with different TiO_2-NPs content for 72 h. Representative micrographs of the HSF cell culture of the control group (**a**) and the culture cultivated in the presence of the composite material containing 0.1 wt% TiO_2-NPs (**b**). (**c**) Results of the viability assessment of cell cultures. Data are presented as mean values ± SEM (n = 3). The scale bar in the lower right corner represents 10 μm.

3. Discussion

The growing interest in TiO_2-NPs is due to their high antibacterial potential against bacteria, including antibiotic-resistant bacteria. In this regard, TiO_2-NPs can be an effective tool in healthcare, the food industry, the production of materials for the tropics, and environmental protection [37,38]. The incorporation of titanium dioxide (TiO_2) nanoparticles into polymer matrices is a promising direction in materials science due to the unique properties of TiO_2, such as photocatalytic activity [39], resistance to UV radiation [40], antibacterial action [41], and increased mechanical strength. Colloidal solutions of TiO_2-NPs were synthesized using laser ablation and subsequent laser sintering. The synthesized nanoparticle samples had a shape close to spherical (Figure 1a), the surface morphology was knobby, the average size was ~150 nm (Figure 1b), the optical absorption spectrum corresponded to titanium dioxide (Figure 1c), and the maximum of the ζ-potential distribution was −30 mV (Figure 1d), which determined the stability of the colloidal solution of the synthesized nanoparticles. The obtained colloidal solution of TiO_2-NPs was added to methacrylate photopolymer resin (MPR) at final concentrations of 0.001, 0.01, and 0.1 wt.%. Various samples were printed from the modified methacrylate resins (MPR/TiO_2-NPs) using an MLSA printer (Figure 3a). The addition of TiO_2-NPs to the resin did not affect the accuracy of 3D printing (Figure 3b). This is important because the addition of nanoparticles to experimental or commercial photopolymer resins significantly worsens the printing accuracy [42,43].

The introduction of 0.1 wt.% TiO_2-NPs into the methacrylic polymer matrix, on the one hand, reduces the yield strength of the polymer matrix, and on the other hand, it contributes to an increase in the tensile strength and a change in the deformation nature of the polymer material (Figure 4a,b). A slightly smaller applied force was required to destroy the composite material samples, but a higher resistance to deformation loads was observed compared to the polymer without nanoparticles. This compromise can be explained by the peculiarities of the interaction between TiO_2-NPs and the polymer matrix: on the one hand, TiO_2-NPs improve stress distribution, increase stiffness, and promote strengthening by limiting the mobility of polymer chains and creating additional stress-distribution centers, which leads to an increase in tensile strength [44]. Conversely, the presence of TiO_2-NPs in the matrix can cause local stress concentrations and microdefects that reduce

the resistance to initial plastic deformation, which is manifested by a decrease in the yield strength [45]. Such composites find applications in dentistry, biomedicine, and optics, where high strength and resistance to mechanical stress while maintaining sufficient flexibility and transparency are particularly valuable [46]. For example, in dental restorative materials and orthopedic implants, this allows for the achievement of longer-lasting structures with optimal functional characteristics, despite some loss in initial plasticity [47]. In addition, this behavior of the polymer composite material may be of interest when used in systems where a gradient load is applied [48]. In general, this deformation behavior is consistent with other known materials based on methacrylates with the addition of nanoparticles of complex morphology [49].

The printed round plates made of MPR/TiO_2-NPs were examined using atomic force microscopy after careful polishing. The samples printed from resins containing nanoparticles were polished, similar to the samples without nanoparticles. All samples displayed surface areas measuring 8 × 8 μm, where the surface profile height did not exceed 10 nm (Figure 5a,b). No significant surface defects were observed in the materials, which often arise when nanoparticles are introduced into a polymer matrix [50]. Surface characteristics such as homogeneity and defectlessness are especially important for potential biomedical applications, where surface uniformity plays a key role in interactions with biological tissues [51]. The absence of significant irregularities may also indicate the potential compatibility of the components of the composite material [52]. Modulation interference microscopy was used to assess the distribution of nanoparticles in the polymer matrix [53]. None of the samples contained internal voids, cavities, or other hidden defects. At the same time, a non-uniform distribution of TiO_2-NPs in the volume of the methacrylate polymer matrix was demonstrated (Figure 6a–d). Typically, nanoparticles in a polymer matrix are distributed more uniformly without forming micrometer-sized zones with different local concentrations. At the same time, we found several examples of the gradient filling of polymers with nanoparticles in the literature [54,55]. The degree of dispersion of TiO_2-NPs may depend on factors such as the concentration of nanoparticles in the polymer matrix, type of polymer, interactions at the polymer-nanoparticle interface, and processing (mixing) method [56]. As a rule, higher concentrations of TiO_2-NPs lead to increased agglomeration due to the strong tendency of nanoparticles to aggregate, especially with large surface areas and polarities [57]. The choice of polymer matrix can also determine the dispersibility of the nanoparticles. In turn, polymers can exhibit different interactions with TiO_2-NPs, affecting their dispersion. Some polymers may exhibit a higher affinity for the surface of nanoparticles and promote better dispersion. In particular, polyacrylic and methacrylic polymers with functional groups (carboxyl, hydroxyl, or amino groups) can form more effective bonds with the surface of TiO_2-NPs [58]. The use of binding agents and block copolymers is also intended to improve the dispersibility of TiO_2-NPs in polymer matrices [59,60]. To achieve a uniform distribution of nanoparticles in the polymer volume, several solutions have been proposed, including the functionalization of nanoparticles with groups that improve the affinity with matrix monomers [61,62], the addition of suitable dispersing agents or surfactants [63], modification of the mixing method using mechanical mixing [64], ultrasonic treatment [65], extrusion or high-energy stirring [66], and the use of solvents that ensure temporary compatibility of the components [13].

To evaluate the effect of TiO_2-NPs on the chemical structure of the polymer matrix, as well as to evaluate the effect of the introduction of TiO_2-NPs on the degree of polymerization of the resin, FTIR spectra of the materials (Figure 7a) and absorption spectra in the UV-Vis optical region (Figure 7b) were obtained. One of the key problems in working with methacrylate materials is achieving a high degree of monomer conversion during polymerization [67]. Incomplete conversion of the original components leads to the retention of toxic

methacrylate monomers in the polymer matrix, which is especially dangerous in biomedical applications, such as dentistry, where residual monomers can diffuse through dentinal tubules and have a cytotoxic effect on the dental pulp [68,69]. The original methacrylate resin is a complex system containing methacrylate monomers and oligomers of various molecular weights, as well as polymerization photoinitiators [70]. The key aspect of the curing process is the rupture of the C=C double bonds in the methacrylate groups with the subsequent formation of a polymer network. The observed decrease in the intensity of the bands at 1611 and 1637 cm^{-1} in the IR spectra can serve as a reliable indicator of the degree of completion of the polymerization process, which may indicate the minimal potential toxicity of the resulting composite materials. In addition, the addition of TiO_2-NPs did not significantly affect the spectral characteristics of the photoinitiators, indicating the preservation of the efficiency of the photopolymerization process in the modified materials. In general, the possibility of controlling the degree of polymerization of resins by introducing nanosized fillers is of considerable interest and has been widely discussed in modern studies [71–73]. In particular, it has been reported that nanoparticles increase the overall conversion of monomers through the following mechanisms: NPs can act as centers for additional cross-linking of polymer chains [74], NPs can have a catalytic effect on the polymerization process [75], NPs contribute to changes in the efficiency of UV absorption by photoinitiators [76], and can also affect the mobility of reactive groups [77]. Numerous studies have reported the use of TiO_2-NPs as a functional additive in photopolymer resins to enhance acrylate monomer conversion and, in general, the photopolymerization of materials. TiO_2-NPs enhance the polymerization of photopolymer systems through a combination of several factors. One of the key mechanisms is related to their ability to effectively absorb ultraviolet radiation, especially in the range corresponding to the spectrum of action of polymerization initiators [78]. In turn, the photocatalytic activity of TiO_2-NPs can also lead to the generation of active oxygen species or free radicals on the surface of the nanoparticles, which in turn initiates or enhances the polymerization chain reaction. In addition, TiO_2-NPs exhibit photocatalytic activity, especially in the anatase crystal form, which allows them to accelerate the formation of active polymerization centers under UV irradiation [79,80]. The surface of TiO_2-NPs can also influence the local concentration of monomers and initiators, forming nucleation centers for the polymer chain and creating a microenvironment that promotes a more efficient polymerization reaction [81,82]. These factors contribute to the accelerated, deeper, and more complete polymerization of photosensitive materials.

To study the bioactive properties of polymeric materials, as well as polymer-based composite materials, the ability to form biologically active molecules on the surface, such as reactive oxygen species, is of considerable interest [83]. It is known that reactive oxygen species, on the one hand, play an important signaling and regulatory role in living systems [84], on the other hand, a significant increase in the concentration of reactive oxygen species can lead to the development of oxidative stress [85] and even death [86]. In this regard, the ability of the obtained composite materials to generate hydrogen peroxide and hydroxyl radicals was assessed. The composite material samples exhibited weak pro-oxidant activity (Figure 8a,b). Reactive oxygen species are formed under the action of elevated temperatures via different mechanisms [87]. The obtained results indicate two sources of the origin of reactive oxygen species: on the one hand, a certain contribution is made by the polymer matrix itself, which we assume due to the residual components of photosensitizers; on the other hand, a pronounced enhancement is provided by TiO_2-NPs. The active forms of oxygen, nitrogen, and chlorine often have destructive effects on biomolecules [88–90]. It has been shown that incubation with MPR/TiO_2-NPs in DNA results in more intense formation of 8-oxoguanine (Figure 9a), a key biomarker of oxidative

stress [91]. In addition, in the presence of MPR/TiO_2-NPs, an increase in the level of long-lived reactive protein species was observed (Figure 9b). It is known that LRPS can be a source of active oxygen forms [92]. Antioxidants can prevent the formation of 8-oxoguanine in DNA and neutralize LRPS [93].

Polymer composite materials can prevent the proliferation of bacterial microflora on surfaces [94–96]. To assess the inhibitory activity of the obtained composite materials, the growth kinetics of bacterial cultures of *E. coli* cells continuously in contact with the surfaces of the material samples were studied (Figure 10). All composite materials significantly inhibited the growth of suspension bacterial cultures, while the polymer matrix without the addition of TiO_2-NPs did not exhibit independent bacteriostatic activity. At the same time, significant differences in the duration of the lag phase were observed during growth in the presence of composite materials compared with the values for control cultures and cultures growing in the presence of a polymer without the addition of TiO_2-NPs, which may indicate a mechanism of action of composite materials associated with the inhibition of cell division processes. Flow cytometry with propidium iodide staining of bacterial cells was also used to study the antimicrobial properties of the obtained composite materials (Figure 11). This approach is highly accurate and allows for the differential staining of bacterial cells for a more detailed study of the antibacterial effect [97]. Cytofluorometric studies demonstrated a general decrease in the concentration of bacterial cells in the presence of composite materials and a significant increase in the proportion of non-viable (PI-positive) bacterial cells (Figure 12a,b). The observed bactericidal effect demonstrated a clear correlation between the concentration of nanoparticles and the severity of the antimicrobial effect, reaching maximum values at a TiO_2-NPs content of 0.1 wt.%. The observed pronounced antibacterial effect is probably due to damage to the bacterial membranes [98]. The antibacterial activity of TiO_2-NPs is mediated by several contact mechanisms. It has been shown that TiO_2-NPs, when in contact with the cell membrane, are capable of causing its depolarization, followed by a disruption of its barrier properties [99]. Significant damage to the cell wall of Gram-positive bacteria was also observed due to sorption on the surface of TiO_2-NPs [100]. In the case of TiO_2-NPs exposure to Gram-negative bacteria, the key molecular targets are membrane proteins and lipopolysaccharides (Gram-negative bacteria), and in the case of Gram-positive bacteria, lipoteichoic acids and peptidoglycan. The interaction of TiO_2-NPs with membrane and cell wall components can also be considered an additional factor of exposure, together with photocatalytic reactions [101]. The obtained data complement the results of previous studies, confirming the complex antimicrobial action of the developed composite materials, including bacteriostatic and bactericidal components [102–104]. The results of the microbiological studies are of interest for the development of improved antimicrobial materials and confirm the promise of using the considered composite materials printed from MPR/TiO_2-NPs to create surfaces with controlled antimicrobial properties. Overall, the antibacterial activity of TiO_2-NPs is consistent with other reported results [105,106]. Despite the high degree of antibacterial activity of TiO_2-NPs, in several comparative studies, the antibacterial potential of TiO_2-NPs was lower than that of other nanoparticles. For example, it has been noted that ZnO-NPs have higher antibacterial activity than TiO_2-NPs under the same exposure conditions and concentrations [107–109]. The degree of activity of NPs against bacterial cells is determined by their mechanisms of action; in particular, ZnO NPs, in addition to the characteristic photocatalytic activity of TiO_2-NPs, also exhibit cation-mediated toxicity [110]. Notably, in the absence of UV radiation, the activity of ZnO and TiO_2-NPs decreases and is inferior to that of Ag-NPs [111].

Microscopic studies were performed to assess the cytocompatibility of the studied composite polymer materials with eukaryotic cells (Figure 13a,b). Composite materials con-

taining even the maximum concentration of TiO_2-NPs—0.1 wt.% did not have a significant effect on the morphological characteristics of HSF cell cultures. The results obtained during the viability assessment also indicated good biocompatibility of the composite materials (Figure 13c). The absence of a cytotoxic effect, despite the pronounced antimicrobial activity, makes these materials promising for biomedical applications, where a combination of antiseptic properties and safety for mammalian cells is required [112]. The obtained results are particularly important in the context of the potential use of such composites in areas where a balanced antibacterial effect is required, in combination with biocompatibility and environmental safety.

Thus, the data obtained during this work indicate that the photopolymer methacrylate resin modified by adding TiO_2-NPs is a very effective basis for the additive production of composite materials with improved physicochemical properties and balanced biological activity, which determines the prospects for its use in obtaining functional products that are safe for the environment. For a comprehensive assessment of biocompatibility, durability, and long-term functional effectiveness, in vivo studies on animal models close to the application of the composite materials obtained in real clinical practice are planned.

4. Materials and Methods

4.1. Synthesis of TiO_2 Nanoparticles (TiO_2-NPs)

The titanium dioxide nanoparticles (TiO_2-NPs) of nanometer (~150 nm) size used in this work were obtained by laser sintering of titanium dioxide nanoparticles with an average size of 20 nm in a liquid. Initial titanium dioxide nanoparticles with a size of 20 nm were obtained by laser ablation of a solid metal Ti target (purity 99.99%) in a liquid. Deionized water (0.1 μS/cm) was used as the working liquid, and the volume of the working liquid was 120 mL. The target was attached to the bottom of a 60 mL glass cuvette, and the thickness of the liquid layer on the surface of the target was approximately 3 mm. Using a peristaltic pump, the volume of water in the cuvette was pumped through an additional 60 mL reservoir, providing a constant circulation of liquid in the system. A P-Mark TT 100 ytterbium fiber laser (Pokkels, Moscow, Russia) with a wavelength of 1064 nm, a pulse repetition rate of 35 kHz, a pulse duration of 200 ns, and energy of 1.5 mJ was used as the laser radiation source. Laser radiation was focused on the target surface and moved along it using an LScanH galvano-optical scanning system (Ateko-TM, Moscow, Russia) with an F-Theta lens (focal length of 90 mm). Scanning was performed along straight lines inscribed in a rectangular area with dimensions of 2 × 3 cm at a speed of 3000 mm/s. The distance between adjacent scanning lines was approximately 20 μm. The total duration of the laser ablation was 1 h.

A pulsed Nd:YAG laser NL300 (Ekspla, Vilnius, Lithuania) was used as the source of laser radiation during the sintering of the titanium nanoparticles with the following parameters: pulse duration of 4 ns, repetition rate of 1 kHz, wavelength of 1064 nm, and pulse energy of 0.2 mJ. Laser radiation from a laser source was supplied to the cuvette from below using reflective mirrors and focused at a distance of 2 cm from the bottom of the cuvette. The diameter of the laser spot at the beam waist was 150 μm. Introducing radiation through the bottom of the cuvette allowed us to solve the problem of gas bubbles floating. During repeated irradiation of the colloid, the radiation beam moved through the colloid in a manner similar to that of a scanner system. The sintering time of titanium nanoparticles using laser radiation was about 2 h. After laser sintering, the colloid was centrifuged using a Sigma 3-16KL centrifuge at 7000 rpm for 30 min to separate the nanoparticles obtained by laser sintering from the original smaller nanoparticles.

4.2. Characterization of TiO_2-NPs

The hydrodynamic diameter, ζ-potential, and concentration of nanoparticles were determined using a Malvern Zetasizer Ultra analyzer (Malvern Panalytical Ltd., Malvern, UK) with a 10 × 10 mm quartz cuvette and a 'Dip' Cell ZEN1002 electrode. UV-Vis spectroscopy was performed using a Cintra 4040 spectrophotometer (GBC Scientific Equipment Pty Ltd., Victoria, Australia). The morphology of the nanoparticles was studied using a Libra 200 FE HR transmission electron microscope (TEM) (Carl Zeiss, Jena, Germany). The details of the experiments have been described previously [95].

4.3. Preparation of TiO_2-NPs Modified Photopolymer Resin (MPR/TiO_2-NPs)

The method of integrating TiO_2-NPs into methacrylate photopolymer resin (MPR) consisted of two main steps: preparation of NP dispersions in acetone and direct introduction of TiO_2-NPs into the MPR. TiO_2-NPs dispersions in acetone were obtained by transferring NPs from aqueous dispersions as follows: an aqueous dispersion of TiO_2-NPs was poured equally into two centrifuge tubes, and a centrifugation cycle was performed for 40 min at 22 °C and 7012 rpm using a 3-16KL rotor centrifuge (Sigma, Darmstadt, Germany). The solvent above the precipitated NPs (supernatant) was then collected. Acetone (Komponent-Reaktiv, Moscow, Russia) was added to the precipitated TiO_2-NPs in a glass beaker. The particles were then dispersed in the added solvent: 3–5 min of treatment in an ultrasonic bath (40 kHz, 22 °C) and 3–5 min of shaking using a vortex. A repeated centrifugation cycle was performed, followed by the collection of the solvent, the addition of acetone, and redispersion of the precipitated TiO_2-NPs. The procedure was repeated three times. The resulting dispersion of TiO_2-NPs in acetone was transferred into a glass vial with a screw cap. The resulting colloidal solution of TiO_2-NPs in acetone was mixed with MPR based on methacrylic monomers and oligomers, Dental Clear PRO (Harz Labs, Mytishchi, Russia), to achieve final nanoparticle concentrations of 0.001%, 0.01%, and 0.1% by weight. The original MPR was a transparent liquid with a viscosity of 1000 ± 200 mPa · s. Products printed from this material have high transparency, accuracy, chemical resistance, and autoclaving resistance. The material complies with ISO 10993 [113] and has a registration certificate for a medical device No. RZN 2020/12007. To ensure a uniform distribution of nanoparticles in the resin, two-stage mixing was performed: mechanical mixing on an MS 3 digital shaker (IKA, Wilmington, NC, USA) for 5 min and ultrasonic treatment (40 kHz, 22 °C) for 5 min. The finished samples of MPR modified by the addition of TiO_2-NPs (MPR/TiO_2-NPs) were stored in sealed dark glass bottles (V = 500 mL) in a light-protected place.

4.4. Additive Manufacturing of MPR/TiO_2-NPs Composite Material Samples

A Saturn 3 Ultra 12 K MSLA printer (Elegoo, Shenzhen, China) was used to fabricate the samples. Before printing, the prepared MPR/TiO_2-NPs were poured into the tank. The control samples were made of pure resin without nanoparticles. For each MPR/TiO_2-NPs sample, the following were printed: samples according to ISO 179-1:2010 Type 1 (for impact testing), samples according to ISO 527-2:2012 Type 1A (for mechanical testing), and round plates (⌀16 mm, thickness 0.5 mm) for physicochemical and biological studies.

The number of replicates for each group was $n = 3$.

The printed samples of MPR/TiO_2-NPs composite materials underwent multi-stage post-processing, including primary washing—immersion in absolute isopropanol (99.9%) for 6 min using a magnetic stirrer (UW-02, Creality3D, Shenzhen, China); ultrasonic cleaning—additional treatment in an ultrasonic bath with isopropanol (6 min); drying—holding at room temperature (10 min); finishing treatment—application of glycerol followed by UV curing for 30 min on a rotating platform (UW-02, Creality3D, Shenzhen, China); repeated ultrasonic treatment (6 min) and drying (10 min); and heat treatment—heating in

a drying oven at 80 °C (30 min). The finished samples were stored in closed Petri dishes under standard conditions.

4.5. Methods for Characterization of Composite Materials Printed from MPR/TiO_2-NPs

The micro- and nanostructures of the surface of the printed samples were studied using a morphology analysis complex (NT-MDT, Zelenograd, Russia). Measurements were performed in non-contact and semi-contact modes. The interaction of the nanoparticles with the polymer matrix was studied using an IR-8000 FTIR spectrometer (SAS LLC, Krasnoyarsk, Russia) with a ZnSe Sealed Flat Plate attachment (Pike Technologies, Fitchburg, WI, USA) and a Cintra 4040 dual-beam UV/Vis spectrometer (GBC Scientific Equipment Pty Ltd., Victoria,Australia). The distribution of TiO_2-NPs in the polymer matrix was analyzed using an MIM-321 modulation interference microscope (Amphora Laboratories, Moscow, Russia). Mechanical properties were evaluated on a WDW-5S universal testing machine (Hongtuo,Binzhou, China): tensile tests were performed in accordance with ASTM D638-22, and bending tests were performed in accordance with ASTM D790 (Type 1A, Type B samples according to ISO 527-2:2012). All measurements were performed at ambient temperature. At least five repeated tests were performed for each sample type. The loading rate was 2 mm/min for the tensile tests and 1 mm/min for the bending tests. The obtained data were processed using specialized software supplied with the equipment.

4.6. Quantitative Assessment of the Formed ROS in Aqueous Solutions (H_2O_2 and $^{\bullet}OH$)

The quantitative assessment of the formation of active oxygen species (hydrogen peroxide H_2O_2, and hydroxyl radicals •OH) in aqueous solutions incubated with printed composite materials from MPR/TiO_2-NPs was carried out using specialized analytical methods. The concentration of hydrogen peroxide was determined by chemiluminescence using a highly sensitive chemiluminometer, "Biotox-7A-USE" (Engineering Center-Ecology, Moscow, Russia). Measurements were performed using a reaction system containing luminol, p-iodophenol, and horseradish peroxidase in Tris-HCl buffer (pH 8.5). Composite material samples in the form of films measuring 10 × 10 × 0.5 mm were placed in polypropylene vials filled with distilled water and incubated at 40 °C for 3 h, after which a counting solution containing 1 mM Tris-HCl buffer, 50 μM para-iodophenol, 50 μM luminol, and 10 nM horseradish peroxidase (pH 8.5), prepared immediately before the analysis, was added. The applied technique has exceptional sensitivity, allowing the detection of hydrogen peroxide at concentrations below 0.1 nM. The experimental details have been published previously [114].

A fluorimetric method based on the reaction with coumarin-3-carboxylic acid was used for the quantitative determination of hydroxyl radicals. The studied samples in the form of thin films (10 × 10 × 0.5 mm) were placed in an aqueous solution of CCA with the addition of phosphate buffer and incubated at a strictly controlled temperature of 80.0 ± 0.1 °C for 2 h. The fluorescent product formed during the reaction, 7-hydroxycoumarin-3-carboxylic acid, was recorded using a JASCO 8300 spectrofluorometer (JASCO, Tokyo, Japan) at excitation wavelengths of 400 nm and emission wavelengths of 450 nm. In all experiments, control measurements were performed without samples to exclude background signals. A series of composite material samples with different TiO_2-NPs contents (0.001–0.1 wt.%) were studied; each analysis was performed in triplicate to ensure statistical reliability of the results. The experimental details have been published previously [115].

4.7. Quantitative Determination of 8-Oxoguanine in DNA and Long-Lived Reactive Protein Species (LRPS)

Quantitative analysis of 8-oxoguanine in DNA samples was performed using an enzyme immunoassay with specific monoclonal antibodies. Sample preparation included

the following steps: DNA samples were brought to a concentration of 350 μg/mL, denatured by heating in a water bath (5 min), and then cooled on ice. For the analysis, 42 μL of the prepared DNA was applied to the wells of the plate, where the molecules were immobilized at 80 °C for 3 h. Non-specific binding sites were blocked with a 1% solution of skim milk in Tris-HCl buffer (pH 8.7) with the addition of 0.15 M NaCl (incubated for 14–18 h at room temperature). Next, primary antibodies against 8-oxoguanine (diluted 1:2000) were added to the wells and incubated for 3 h at 37 °C. After washing, horseradish peroxidase-conjugated secondary antibodies (diluted 1:1000) were added and incubated for 1.5 h at 37 °C. The enzymatic reaction was detected using a substrate of 18.2 mM ABTS in the presence of 2.6 mM H_2O_2 in 75 mM citrate buffer (pH 4.2), which was stopped by adding 100 μL of 1.5 mM sodium azide when a color appeared. Optical density was measured at 405 nm using a Feyond-A400 plate reader. The experimental details have been published previously [116].

Composite material samples were used as 10 mm × 10 mm × 0.5 mm plates. The samples were incubated in 10 mL of 0.1% BSA aqueous colloid at 40 °C for 120 min. The LRPS concentration was estimated by recording the chemiluminescence of the protein solutions after incubation at 40 °C for 2 h. After incubation, the samples were kept at room temperature in the dark for 30 min. Measurements were performed in 20 mL polypropylene vials (Beckman, Brea, CA, USA) in complete darkness at room temperature. A highly sensitive Biotox-7A chemiluminometer (Engineering Center—Ecology, Moscow, Russia) was used as the instrument. Bovine serum albumin (BSA) solutions that were not heated were used as controls. All experimental details have been described previously [93].

4.8. E. coli Growth Curves

To study the bacteriostatic properties of the composite materials printed from MPR/TiO_2-NPs, 10 × 10 mm samples were prepared and placed in the wells of a 24-well plate. The samples were pre-treated with 70% ethanol (1 mL per well), followed by UV sterilization in a laminar flow hood for 40 min. In parallel, a bacterial suspension of *E. coli* was prepared by transferring a colony of bacteria into 10 mL of sterile LB broth using a sterile loop and culturing it in a shaker incubator at 37 °C and 230 rpm overnight. Before the experiment, the overnight culture was diluted 1000-fold with fresh broth to a concentration of approximately 10^6 CFU/mL, and BNP was thoroughly mixed on a V-1 Plus vortexer (Biosan, Rīga, Latvia). The resulting bacterial suspension (1000 μL) was added to each well containing a material sample, after which the plate without a lid was placed in a plate photometer equipped with a thermostat and a shaking system. After 24 h at a constant temperature of 37 °C and shaking every hour, the optical density of bacterial cultures at a wavelength of 600 nm (OD600) was measured. Based on the data obtained, growth curves were constructed to analyze the effect of the obtained materials on the duration of the lag phase, rate of exponential growth, and maximum density of bacterial cultures. Pure polymer without the addition of TiO_2-NPs and sterile broth without bacteria were used as controls. All experiments were performed in triplicate.

4.9. Evaluation of Antibacterial Activity by Flow Cytofluorometry

For a more detailed study of the antibacterial action of composite materials printed from MPR/TiO_2-NPs, flow cytometry was additionally performed using a Longcyte cytofluorimeter (Challenbio, Beijing, China). *E. coli* bacterial cultures were prepared and cultivated in the presence of the studied samples according to a previously described method. After completion of the cultivation process, 1 mL of phosphate-buffered saline (PBS) manufactured by Sigma-Aldrich (St. Louis, MO, USA) containing 4 μM propidium iodide (PI), Lumiprobe (Cockeysville, MD, USA) was added to each well of a 24-well plate. After

adding the dye, the plate was incubated for 60 min in the complete absence of light to allow complete binding. Before analysis, the samples were carefully resuspended and transferred to sterile 1.5 mL Expell Microcentrifuge Tubes (Capp, Nordhausen, Germany), which were then placed in a cytofluorimeter stand for subsequent measurements. For each sample, event counting, side (SS) and forward (FS) light scattering, and propidium iodide (PI) fluorescence intensity were assessed. Fluorescence was recorded in the orange-red channel with an excitation maximum at 535 nm and an emission maximum at 617 nm, which allowed for the accurate determination of the number of damaged bacterial cells with impaired membrane integrity. To assess the concentration of bacteria in the suspension, an automated recalculation of the number of events per 1 mL of suspension was performed. The bactericidal effect was assessed based on the proportion of dead cells. The proportion of dead cells was assessed using the threshold method by setting the gate boundaries based on the geometric mean of PI fluorescence intensity in control samples without the presence of polymers and composite materials.

4.10. Cytotoxicity Assessment In Vitro

The biocompatibility of the printed MPR/TiO_2-NPs composites was studied using a culture of human spleen fibroblasts (HSF) purchased from ScienCell (#5530, ScienCell, Carlsbad, CA, USA). The cells were cultured under standard conditions using a DMEM/F12 nutrient medium supplemented with 10% fetal bovine serum, 2 mM L-glutamine, and antibiotics (25 U/mL penicillin and 25 μg/mL streptomycin). Before the experiment, round cover glasses (25 mm in diameter) were sterilized at 180 °C for 2 h. A cell suspension at a density of 105 cells in 200 μL of medium was applied to the prepared glass slides, which were placed in the wells of a 6-well plate. To ensure cell adhesion, the plate was incubated for 30 min in a S-Bt Smart Biotherm CO_2 incubator (Biosan, Rīga, Latvia) at 37 °C and 5% CO_2. Then, 1800 μL of fresh nutrient medium was added to each well, and the tested samples of the composite materials were placed. The cultivation was continued for 72 h under controlled conditions. After incubation, the samples were removed, and microscopic analysis of the cell cultures was performed. A combination of fluorescent dyes was used to assess cell viability: Hoechst 33342 for staining the nuclei, rhodamine for visualizing mitochondria, and propidium iodide for detecting dead cells. A DMI 4000B system was used to visualize and record the cells, and the resulting images were analyzed using ImageJ software v.2.14.0. Each experimental variant was repeated five times to ensure the statistical reliability of the results. All experimental details have been described previously [117].

4.11. Statistical Data Analysis and Visualization

Experimental data processing and statistical analyses were performed using GraphPad Prism 8.3.0 software. Results are presented as mean values ± standard error of the mean. The results from at least three independent experiments were averaged.

5. Conclusions

Thus, in this work, titanium oxide (TiO_2-NPs) nanoparticles with a complex surface topology were obtained for the first time using simple laser sintering procedures. A composite material (MPR/TiO_2-NPs) for 3D printing using MSLA technology was created based on the obtained nanoparticles and a photopolymer resin, such as polymethylmethacrylate. Products made of a material containing 0.001–0.1% by weight of TiO_2-NPs did not contain internal defects and were less brittle than the resin without nanoparticles. Products made of MPR/TiO_2-NPs material are highly polished. After polishing, areas with a variation in the height of the surface profile of less than 10 nm were observed on the surfaces of the products. The nanoparticles were unevenly distributed in the volume of the products. Mod-

ulation interference microscopy revealed alternating regions of several micrometers in size, which were clearly distinguishable from each other, with slightly higher and slightly lower concentrations of TiO_2-NPs. Spectroscopy has shown that the addition of titanium oxide nanoparticles promotes better polymerization of MPR resin. Upon contact with aqueous solutions, the resulting material exhibits a weak ability to generate reactive oxygen species. At the same time, the resulting material exhibits pronounced antibacterial properties and does not affect the growth and reproduction of animal cells. The created material can serve as a highly effective basis for the additive manufacturing of products with improved physicochemical properties and balanced biological activity.

Author Contributions: Conceptualization, A.V.S. and S.V.G.; methodology, A.V.S.; software, M.E.A.; investigation, A.V.S., D.E.B., I.V.B., A.V.G., D.A.S., P.C., S.Z.V., and F.M.Y.; writing—original draft preparation, A.V.S. and D.E.B.; writing—review and editing, S.V.G.; visualization, I.V.B.; supervision, S.V.G. All authors have read and agreed to the published version of the manuscript.

Funding: This research was funded by a grant from the Ministry of Science and Higher Education of the Russian Federation, grant number 075-15-2024-646.

Institutional Review Board Statement: Not applicable.

Informed Consent Statement: Not applicable.

Data Availability Statement: The raw data supporting the conclusions of this article will be made available by the authors upon request.

Acknowledgments: The authors thank the Center for Collective Use of the GPI RAS.

Conflicts of Interest: Author Pavel Chapala was employed by the company HARZ Labs LLC. The remaining authors declare that the research was conducted in the absence of any commercial or financial relationships that could be construed as a potential conflict of interest.

Abbreviations

The following abbreviations are used in this manuscript:

ROS	Reactive Oxygen Species
LRPS	Long-lived Reactive Protein Species
OD	Optical Density
PI	Propidium Iodide
TiO_2-NPs	Titanium oxide nanoparticles
MPR	Methacrylate-like Photopolymer Resin
MSLA	Masked Stereolithography Apparatus

References

1. Che Ab Rahman, A.; Lee, B.-J.; Lim, S. Optimizing polymethyl methacrylate (PMMA)-based stretchable microneedle arrays by vat photopolymerization for efficient drug loading. *Addit. Manuf.* **2024**, *94*, 104472. [CrossRef]
2. Yüceer, Ö.M.; Kaynak Öztürk, E.; Çiçek, E.S.; Aktaş, N.; Bankoğlu Güngör, M. Three-Dimensional-Printed Photopolymer Resin Materials: A Narrative Review on Their Production Techniques and Applications in Dentistry. *Polymers* **2025**, *17*, 316. [CrossRef]
3. Saramet, V.; Stan, M.S.; Ripszky Totan, A.; Țâncu, A.M.C.; Voicu-Balasea, B.; Enasescu, D.S.; Rus-Hrincu, F.; Imre, M. Analysis of Gingival Fibroblasts Behaviour in the Presence of 3D-Printed versus Milled Methacrylate-Based Dental Resins—Do We Have a Winner? *J. Funct. Biomater.* **2024**, *15*, 147. [CrossRef]
4. Zhou, Z.-X.; Hu, W.; Zhao, Z.; Fu, H. Photochemically Driven Polymeric Biocompatible and Antimicrobial Thiol–Acrylate Nanocomposite Suitable for Dental Restoration. *ACS Appl. Mater. Interfaces* **2022**, *14*, 46313–46323. [CrossRef]
5. Manoukakis, T.; Nikolaidis, A.K.; Koulaouzidou, E.A. Polymerization kinetics of 3D-printed orthodontic aligners under different UV post-curing conditions. *Prog. Orthod.* **2024**, *25*, 42. [CrossRef]
6. Zhao, Y.; Wang, Z.; Zhao, J.; Hussain, M.; Wang, M. Additive Manufacturing in Orthopedics: A Review. *ACS Biomater. Sci. Eng.* **2022**, *8*, 1367–1380. [CrossRef]

7. Onderková, A.; Kalaskar, D.M. 3D bioprinting for auricular reconstruction: A review and future perspectives. *Int. J. Bioprinting* **2023**, *9*, 0898. [CrossRef]
8. Alrahlah, A.; Fouad, H.; Hashem, M.; Niazy, A.A.; AlBadah, A. Titanium Oxide (TiO_2)/Polymethylmethacrylate (PMMA) Denture Base Nanocomposites: Mechanical, Viscoelastic and Antibacterial Behavior. *Materials* **2018**, *11*, 1096. [CrossRef]
9. Gad, M.M.; Abualsaud, R. Behavior of PMMA Denture Base Materials Containing Titanium Dioxide Nanoparticles: A Literature Review. *Int. J. Biomater.* **2019**, *2019*, 6190610. [CrossRef]
10. Mhaibes, A.H.; Safi, I.N.; Haider, J. The influence of the addition of titanium oxide nanotubes on the properties of 3D printed denture base materials. *J. Esthet. Restor. Dent.* **2024**, *36*, 1574–1590. [CrossRef]
11. Chen, S.; Yang, J.; Li, K.; Lu, B.; Ren, L. Carboxylic acid-functionalized TiO_2 nanoparticle-loaded PMMA/PEEK copolymer matrix as a dental resin for 3D complete denture manufacturing by stereolitographic technique. *Int. J. Food Prop.* **2018**, *21*, 2557–2565. [CrossRef]
12. Mohr, L.C.; Capelezzo, A.P.; Baretta, C.R.D.M.; Martins, M.A.P.M.; Fiori, M.A.; Mello, J.M.M. Titanium dioxide nanoparticles applied as ultraviolet radiation blocker in the polylactic acid bidegradable polymer. *Polym. Test.* **2019**, *77*, 105867. [CrossRef]
13. Cazan, C.; Enesca, A.; Andronic, L. Synergic Effect of TiO_2 Filler on the Mechanical Properties of Polymer Nanocomposites. *Polymers* **2021**, *13*, 2017. [CrossRef] [PubMed]
14. Zuniga, J.M. 3D Printed Antibacterial Prostheses. *Appl. Sci.* **2018**, *8*, 1651. [CrossRef]
15. Marin, E.; Boschetto, F.; Zanocco, M.; Honma, T.; Zhu, W.; Pezzotti, G. Explorative study on the antibacterial effects of 3D-printed PMMA/nitrides composites. *Materials & Design* **2021**, *206*, 109788. [CrossRef]
16. Serov, D.A.; Gritsaeva, A.V.; Yanbaev, F.M.; Simakin, A.V.; Gudkov, S.V. Review of Antimicrobial Properties of Titanium Dioxide Nanoparticles. *Int. J. Mol. Sci.* **2024**, *25*, 10519. [CrossRef]
17. Manimaran, K.; Loganathan, S.; Prakash, D.G.; Natarajan, D. Antibacterial and anticancer potential of mycosynthesized titanium dioxide (TiO_2) nanoparticles using *Hypsizygus ulmarius*. *Biomass Convers. Biorefinery* **2022**, *14*, 13293–13301. [CrossRef]
18. Dilika, M.D.; Fanta, G.M.; Tański, T. Green Synthesis of Titanium Dioxide Nanoparticles Using Maerua oblongifolia Root Bark Extract: Photocatalytic Degradation and Antibacterial Activities. *Materials* **2024**, *17*, 5835. [CrossRef]
19. Bano, F. Green-Synthesized Titanium Dioxide Nanoparticles Inhibit and Eradicate the Biofilms of Pathogenic Bacteria Through Intracellular ROS Production. *Microbiol. Res.* **2025**, *16*, 48. [CrossRef]
20. Nosrati, H.; Heydari, M. Titanium dioxide nanoparticles: A promising candidate for wound healing applications. *Burn. Trauma* **2025**, *13*, tkae069. [CrossRef]
21. Zuo, F.; Zhu, Y.; Wu, T.; Li, C.; Liu, Y.; Wu, X.; Ma, J.; Zhang, K.; Ouyang, H.; Qiu, X.; et al. Titanium Dioxide Nanomaterials: Progress in Synthesis and Application in Drug Delivery. *Pharmaceutics* **2024**, *16*, 1214. [CrossRef] [PubMed]
22. Goto, T.; Tanabe, R.; Shibuya, H.; Tamura, M.; Nomura, S.; Chen, J.-C. Visualization of Small Vessels by Micro–Computed Tomography Using Titanium Dioxide Nanoparticles as a Novel Contrast Agent. *Int. J. Biomed. Imaging* **2025**, *2025*, 6688558. [CrossRef]
23. Picolotto, A.; Rossa Beltrami, L.V.; Dallé, D.; Ornaghi Júnior, H.L.; Zattera, A.J.; Catto, A.L.; Borsoi, C. Development and evaluation of biodegradable starch-based films containing cellulose nanocrystals/titanium dioxide nanoparticles as an alternative for food packaging. *J. Thermoplast. Compos. Mater.* **2023**, *37*, 1991–2012. [CrossRef]
24. Wang, J.; Cheng, Y.; Li, S.; Liu, B.; Yang, L.; Geng, F.; Xie, S.; Qi, R.; Zhang, Y.; Liu, D.; et al. Enhanced properties of gelatin films incorporated with TiO_2-loaded reduced graphene oxide aerogel microspheres for active food packaging applications. *Int. J. Biol. Macromol.* **2024**, *261*, 129772. [CrossRef]
25. Chandoliya, R.; Sharma, S.; Sharma, V.; Joshi, R.; Sivanesan, I. Titanium Dioxide Nanoparticle: A Comprehensive Review on Synthesis, Applications and Toxicity. *Plants* **2024**, *13*, 2964. [CrossRef]
26. Gojzewski, H.; Guo, Z.; Grzelachowska, W.; Ridwan, M.G.; Hempenius, M.A.; Grijpma, D.W.; Vancso, G.J. Layer-by-Layer Printing of Photopolymers in 3D: How Weak is the Interface? *ACS Appl. Mater. Interfaces* **2020**, *12*, 8908–8914. [CrossRef]
27. Rao, J.P.; Geckeler, K.E. Polymer nanoparticles: Preparation techniques and size-control parameters. *Prog. Polym. Sci.* **2011**, *36*, 887–913. [CrossRef]
28. Beach, M.A.; Nayanathara, U.; Gao, Y.; Zhang, C.; Xiong, Y.; Wang, Y.; Such, G.K. Polymeric Nanoparticles for Drug Delivery. *Chem. Rev.* **2024**, *124*, 5505–5616. [CrossRef]
29. Georgeous, J.; AlSawaftah, N.; Abuwatfa, W.H.; Husseini, G.A. Review of Gold Nanoparticles: Synthesis, Properties, Shapes, Cellular Uptake, Targeting, Release Mechanisms and Applications in Drug Delivery and Therapy. *Pharmaceutics* **2024**, *16*, 1332. [CrossRef]
30. Baimler, I.V.; Simakin, A.V.; Dorokhov, A.S.; Gudkov, S.V. Mini-review on laser-induced nanoparticle heating and melting. *Front. Chem.* **2024**, *12*, 1463612. [CrossRef]
31. Amendola, V.; Meneghetti, M. Laser ablation synthesis in solution and size manipulation of noble metal nanoparticles. *Phys. Chem. Chem. Phys.* **2009**, *11*, 3805–3821. [CrossRef] [PubMed]

32. Zhang, J.; Claverie, J.; Chaker, M.; Ma, D. Colloidal Metal Nanoparticles Prepared by Laser Ablation and their Applications. *ChemPhysChem* **2017**, *18*, 986–1006. [CrossRef] [PubMed]
33. *ISO 179-1:2010*; Plastics—Determination of Charpy Impact Properties—Part 1: Non-Instrumented Impact Test. ISO: Geneva, Switzerland, 2010.
34. *ISO 527-2:2012*; Plastics–Determination of Tensile Properties. ISO: Geneva, Switzerland, 2012.
35. *ASTM D790*; Standard Test Methods for Flexural Properties of Unreinforced and Reinforced Plastics and Electrical Insulating Materials. ASTM Intemational: West Conshohocken, PA, USA, 1997.
36. *ASTM D638-14*; Standard Test Method for Tensile Properties of Plastics. ASTM International: West Conshohocken, PA, USA, 1998.
37. Arora, B.; Murar, M.; Dhumale, V. Antimicrobial potential of TiO_2 nanoparticles against MDRPseudomonas aeruginosa. *J. Exp. Nanosci.* **2014**, *10*, 819–827. [CrossRef]
38. Ul-Hamid, A.; Baig, N.; Haider, A.; Hakeem, A.S.; Ikram, M. Using biologically synthesized TiO_2 nanoparticles as potential remedy against multiple drug resistant *Staphylococcus aureus* of bovine mastitis. *Sci. Rep.* **2023**, *13*, 18785. [CrossRef]
39. Thakur, N.; Thakur, N.; Kumar, A.; Thakur, V.K.; Kalia, S.; Arya, V.; Kumar, A.; Kumar, S.; Kyzas, G.Z. A critical review on the recent trends of photocatalytic, antibacterial, antioxidant and nanohybrid applications of anatase and rutile TiO_2 nanoparticles. *Sci. Total. Environ.* **2024**, *914*, 169815. [CrossRef]
40. Thuc, D.Q.; Mai, Q.-D.; Son, N.A.; Nguyen, H.A.; Pham, A.-T.; Le, A.-T. Superior UV Resistance of Unsaturated Polyester Resin by Employing Amorphous e-TiO_2 Nanoparticles for Outdoor Applications. *ACS Appl. Polym. Mater.* **2024**, *6*, 3179–3191. [CrossRef]
41. Shabalina, A.V.; Kozlov, V.A.; Popov, I.A.; Gudkov, S.V. A Review on Recently Developed Antibacterial Composites of Inorganic Nanoparticles and Non-Hydrogel Polymers for Biomedical Applications. *Nanomaterials* **2024**, *14*, 1753. [CrossRef]
42. Eren, O.; Yüksel, N.; Şahin, İ. Investigation of mechanical and electrical properties of photopolymer nanocomposites reinforced with carbon-based nanoparticles produced by digital light processing 3D printing technique. *Polym. Compos.* **2024**, *46*, 4729–4742. [CrossRef]
43. Lee, T.; Ng, C.S.; Su, P.-C. Warpage correction for vat photopolymerization 3D printing. *Addit. Manuf.* **2025**, *102*, 104740. [CrossRef]
44. Bangera, M.K.; Kotian, R.; Ravishankar , N. Effect of titanium dioxide nanoparticle reinforcement on flexural strength of denture base resin: A systematic review and meta-analysis. *Jpn. Dent. Sci. Rev.* **2020**, *56*, 68–76. [CrossRef]
45. Shirkavand, S.; Moslehifard, E. Effect of TiO_2 Nanoparticles on Tensile Strength of Dental Acrylic Resins. *J. Dent. Res. Dent. Clin. Dent. Prospect.* **2014**, *8*, 197–203. [CrossRef]
46. Rahman, M.M.; Khan, K.H.; Parvez, M.M.H.; Irizarry, N.; Uddin, M.N. Polymer Nanocomposites with Optimized Nanoparticle Dispersion and Enhanced Functionalities for Industrial Applications. *Processes* **2025**, *13*, 994. [CrossRef]
47. Cascione, M.; De Matteis, V.; Pellegrino, P.; Albanese, G.; De Giorgi, M.L.; Paladini, F.; Corsalini, M.; Rinaldi, R. Improvement of PMMA Dental Matrix Performance by Addition of Titanium Dioxide Nanoparticles and Clay Nanotubes. *Nanomaterials* **2021**, *11*, 2027. [CrossRef] [PubMed]
48. Liang, Y.; Wei, X.; Peng, Y.; Wang, X.; Niu, X. A review on recent applications of machine learning in mechanical properties of composites. *Polym. Compos.* **2024**, *46*, 1939–1960. [CrossRef]
49. Liu, Y.; Wang, Z.; Liu, X.; Chen, H.; Huang, Y.; Li, A.; Pu, Y.; Guo, L. Study on Mechanical Properties, Optical Properties, Cytotoxicity of TiO_2-HAP Nanoparticles-Modified PMMA and Photodynamically Assisted Antibacterial Activity Against Candida Albicans in Vitro. *Int. J. Nanomed.* **2025**, *20*, 2695–2709. [CrossRef]
50. Shayan, M.; Jung, Y.; Huang, P.-S.; Moradi, M.; Plakseychuk, A.Y.; Lee, J.-K.; Shankar, R.; Chun, Y. Improved osteoblast response to UV-irradiated PMMA/TiO_2 nanocomposites with controllable wettability. *J. Mater. Sci. Mater. Med.* **2014**, *25*, 2721–2730. [CrossRef]
51. Ramakrishna, S.; Mayer, J.; Wintermantel, E.; Leong, K.W. Biomedical applications of polymer-composite materials: A review. *Compos. Sci. Technol.* **2001**, *61*, 1189–1224. [CrossRef]
52. Songpanit, M.; Boonyarattanakalin, K.; Limwichean, S.; Lertvanithphol, T.; Horprathum, M.; Pecharapa, W.; Mekprasart, W. Structural and Optical Characterizations of Polymethyl Methacrylate Films with the Incorporation of Ultrafine SiO_2/TiO_2 Composites Utilized as Self-Cleaning Surfaces. *Polymers* **2023**, *15*, 3162. [CrossRef]
53. Ignatyev, P.S.; Indukaev, K.V.; Osipov, P.A.; Sergeev, I.K. Laser Interference Microscopy for Nanobiotechnologies. *Biomed. Eng.* **2013**, *47*, 32–35. [CrossRef]
54. Arrachart, G.; Karatchevtseva, I.; Heinemann, A.; Cassidy, D.J.; Triani, G. Synthesis and characterisation of nanocomposite materials prepared by dispersion of functional TiO_2 nanoparticles in PMMA matrix. *J. Mater. Chem.* **2011**, *21*, 13040–13046. [CrossRef]
55. Azmy, E.; Al-kholy, M.R.Z.; Al-Thobity, A.M.; Gad, M.M.; Helal, M.A.; Chen, W.-C. Comparative Effect of Incorporation of ZrO_2, TiO_2, and SiO_2 Nanoparticles on the Strength and Surface Properties of PMMA Denture Base Material: An In Vitro Study. *Int. J. Biomater.* **2022**, *2022*, 1–10. [CrossRef]

56. Feng, J.; Venna, S.R.; Hopkinson, D.P. Interactions at the interface of polymer matrix-filler particle composites. *Polymer* **2016**, *103*, 189–195. [CrossRef]
57. Takeda, M.; Tanabe, E.; Iwaki, T.; Yabuki, A.; Okuyama, K. High-concentration Transparent TiO_2 Nanocomposite Films Prepared from TiO_2 Nanoslurry Dispersed by Using Bead Mill. *Polym. J.* **2008**, *40*, 694–699. [CrossRef]
58. Lu, K. Hybrid materials—A review on co-dispersion, processing, patterning, and properties. *Int. Mater. Rev.* **2019**, *65*, 463–501. [CrossRef]
59. Charpentier, P.A.; Burgess, K.; Wang, L.; Chowdhury, R.R.; Lotus, A.F.; Moula, G. Nano-TiO_2/polyurethane composites for antibacterial and self-cleaning coatings. *Nanotechnology* **2012**, *23*, 425606. [CrossRef]
60. Chen, X. Preparation and property of TiO_2 nanoparticle dispersed polyvinyl alcohol composite materials. *J. Mater. Sci. Lett.* **2002**, *21*, 1637–1639. [CrossRef]
61. Byrne, M.T.; McCarthy, J.E.; Bent, M.; Blake, R.; Gun'ko, Y.K.; Horvath, E.; Konya, Z.; Kukovecz, A.; Kiricsi, I.; Coleman, J.N. Chemical functionalisation of titania nanotubes and their utilisation for the fabrication of reinforced polystyrene composites. *J. Mater. Chem.* **2007**, *17*, 2351–2358. [CrossRef]
62. Hasan, M.K.; Khan, M.S.; Hossain, M.S.; Dutta, S.K.; Dhar, P.K.; Kawaguchi, S. Polymer encapsulation of TiO_2 by seeded emulsion polymerization to improve the dispersion stability and reflectance. *Colloids Surf. A Physicochem. Eng. Asp.* **2025**, *709*, 136185. [CrossRef]
63. Hanemann, T.; Szabó, D.V. Polymer-Nanoparticle Composites: From Synthesis to Modern Applications. *Materials* **2010**, *3*, 3468–3517. [CrossRef]
64. Nawaz, H.; Umar, M.; Maryam, R.; Nawaz, I.; Razzaq, H.; Malik, T.; Liu, X. Polymer Nanocomposites Based on TiO_2as a Reinforcing Agent: An Overview. *Adv. Eng. Mater.* **2022**, *24*, 2200844. [CrossRef]
65. Wang, C.; Mao, H.; Wang, C.; Fu, S. Dispersibility and Hydrophobicity Analysis of Titanium Dioxide Nanoparticles Grafted with Silane Coupling Agent. *Ind. Eng. Chem. Res.* **2011**, *50*, 11930–11934. [CrossRef]
66. Fonseca, C.; Ochoa, A.; Ulloa, M.T.; Alvarez, E.; Canales, D.; Zapata, P.A. Poly(lactic acid)/TiO_2 nanocomposites as alternative biocidal and antifungal materials. *Mater. Sci. Eng. C* **2015**, *57*, 314–320. [CrossRef]
67. Gziut, K.; Kowalczyk, A.; Schmidt, B.; Idzik, T.J.; Sośnicki, J.G. Influence of Methacrylate and Vinyl Monomers on Radical Bulk Photopolymerization Process and Properties of Epoxy-Acrylate Structural Adhesives. *Polymers* **2023**, *15*, 926. [CrossRef] [PubMed]
68. Leggat, P.A.; Kedjarune, U. Toxicity of methyl methacrylate in dentistry. *Int. Dent. J.* **2003**, *53*, 126–131. [CrossRef]
69. Mohammadi, N.B.; Gerdroudbar, A.E.; Rezazadeh, H.; Mishra, M.K. Plastics and Their Toxicity: Bisphenol A, Phthalate, and Acrylic Monomers for Dental and Pharmaceutical Applications. In *Plastics and Their Toxicity: Bisphenol A, Phthalate, and Acrylic Monomers for Dental and Pharmaceutical Applications*; CRC Press: Boca Raton, FL, USA, 2025.
70. Rudenko, Y.; Lozovaya, A.; Asanova, L.; Fedyakova, N.; Chapala, P. Light intensity influence on critical energy and penetration depth for vat photopolymerization technology. *Prog. Addit. Manuf.* **2023**, *9*, 553–561. [CrossRef]
71. Peng, X.; Zhang, J.; Xiao, P. Photopolymerization Approach to Advanced Polymer Composites: Integration of Surface-Modified Nanofillers for Enhanced Properties. *Adv. Mater.* **2024**, *36*, e2400178. [CrossRef]
72. Shah, M.; Ullah, A.; Azher, K.; Rehman, A.U.; Juan, W.; Aktürk, N.; Tüfekci, C.S.; Salamci, M.U. Vat photopolymerization-based 3D printing of polymer nanocomposites: Current trends and applications. *RSC Adv.* **2023**, *13*, 1456–1496. [CrossRef]
73. Armentia, S.L.d.; Fernández-Villamarín, S.; Ballesteros, Y.; C. del Real, J.; Dunne, N.; Paz, E. 3D Printing of a Graphene-Modified Photopolymer Using Stereolithography for Biomedical Applications: A Study of the Polymerization Reaction. *Int. J. Bioprinting* **2022**, *8*, 182–197. [CrossRef]
74. Cui, W.; Liu, J.; You, W.; Yu, W. Mechanical reinforcement by bridging chains in polymer nanocomposites. *Polymer* **2024**, *306*, 127208. [CrossRef]
75. Melinte, V.; Buruiana, T.; Rosca, I.; Chibac, A.L. TiO_2-Based Photopolymerized Hybrid Catalysts with Visible Light Catalytic Activity Induced by In Situ Generated Ag/Au NPs. *ChemistrySelect* **2019**, *4*, 5138–5149. [CrossRef]
76. Naor, T.; Gigi, S.; Waiskopf, N.; Jacobi, G.; Shoshani, S.; Kam, D.; Magdassi, S.; Banin, E.; Banin, U. ZnO Quantum Photoinitiators as an All-in-One Solution for Multifunctional Photopolymer Nanocomposites. *ACS Nano* **2023**, *17*, 20366–20375. [CrossRef]
77. Bailey, E.J.; Winey, K.I. Dynamics of polymer segments, polymer chains, and nanoparticles in polymer nanocomposite melts: A review. *Prog. Polym. Sci.* **2020**, *105*, 101242. [CrossRef]
78. Mohammadi, H.; Moradpoor, H.; Beddu, S.; Mozaffari, H.R.; Sharifi, R.; Rezaei, R.; Fallahnia, N.; Ebadi, M.; Mazlan, S.A.; Safaei, M. Current trends and research advances on the application of TiO_2 nanoparticles in dentistry: How far are we from clinical translation? *Heliyon* **2025**, *11*, e42169. [CrossRef] [PubMed]
79. Sun, J.; Watson, S.S.; Allsopp, D.A.; Stanley, D.; Skrtic, D. Tuning photo-catalytic activities of TiO_2 nanoparticles using dimethacrylate resins. *Dent. Mater.* **2016**, *32*, 363–372. [CrossRef] [PubMed]

80. Maher, M.A.; Becker-Willinger, C.; Chiao, J.-C.; Schmitz-Stöwe, S.; Bentz, D.; Resnick, P.J.; Veith, M. Kinetic investigations on TiO_2 nanoparticles as photo initiators for UV-polymerization in acrylic matrix. In Proceedings of the Micromachining and Microfabrication Process Technology XV, San Francisco, CA, USA, 26 January 2010.
81. Rocheva, V.V.; Koroleva, A.V.; Savelyev, A.G.; Khaydukov, K.V.; Generalova, A.N.; Nechaev, A.V.; Guller, A.E.; Semchishen, V.A.; Chichkov, B.N.; Khaydukov, E.V. High-resolution 3D photopolymerization assisted by upconversion nanoparticles for rapid prototyping applications. *Sci. Rep.* **2018**, *8*, 3663. [CrossRef]
82. Benites, A.B.; Alarcon, R.T.; Gaglieri, C.; Lamb, K.J.; Bannach, G. Effect of metal oxide fillers in urethane dimethacrylate polymer with glycerol obtained by photopolymerization synthesis. *J. Polym. Res.* **2020**, *27*, 311. [CrossRef]
83. Dube, E. Antimicrobial Photodynamic Therapy: Self-Disinfecting Surfaces for Controlling Microbial Infections. *Microorganisms* **2024**, *12*, 1573. [CrossRef]
84. Tauffenberger, A.; Magistretti, P.J. Reactive Oxygen Species: Beyond Their Reactive Behavior. *Neurochem. Res.* **2021**, *46*, 77–87. [CrossRef]
85. Sharapov, M.G.; Gudkov, S.V.; Lankin, V.Z. Hydroperoxide-Reducing Enzymes in the Regulation of Free-Radical Processes. *Biochemistry* **2021**, *86*, 1256–1274. [CrossRef]
86. Gudkov, S.V.; Gudkova, O.Y.; Chernikov, A.V.; Bruskov, V.I. Protection of mice against X-ray injuries by the post-irradiation administration of guanosine and inosine. *Int. J. Radiat. Biol.* **2009**, *85*, 116–125. [CrossRef]
87. Bruskov, V.I.; Chernikov, A.V.; Ivanov, V.E.; Karmanova, E.E.; Gudkov, S.V. Formation of the Reactive Species of Oxygen, Nitrogen, and Carbon Dioxide in Aqueous Solutions under Physical Impacts. *Phys. Wave Phenom.* **2020**, *28*, 103–106. [CrossRef]
88. Abdal Dayem, A.; Hossain, M.; Lee, S.; Kim, K.; Saha, S.; Yang, G.-M.; Choi, H.; Cho, S.-G. The Role of Reactive Oxygen Species (ROS) in the Biological Activities of Metallic Nanoparticles. *Int. J. Mol. Sci.* **2017**, *18*, 120. [CrossRef]
89. Khramova, Y.V.; Katrukha, V.A.; Chebanenko, V.V.; Kostyuk, A.I.; Gorbunov, N.P.; Panasenko, O.M.; Sokolov, A.V.; Bilan, D.S. Reactive Halogen Species: Role in Living Systems and Current Research Approaches. *Biochemistry* **2024**, *89*, S90–S111. [CrossRef] [PubMed]
90. Menshchikova, E.B.; Khrapova, M.V.; Kozhin, P.M.; Chechushkov, A.V.; Petrova, E.S.; Serykh, A.E.; Romakh, L.P.; Kandalintseva, N.V. Original synthetic monophenolic antioxidant with combined effect inhibits tumor growth in vivo. *Sib. Sci. Med. J.* **2025**, *44*, 128–137. [CrossRef]
91. Kruchinin, A.A.; Kamzeeva, P.N.; Zharkov, D.O.; Aralov, A.V.; Makarova, A.V. 8-Oxoadenine: A «New» Player of the Oxidative Stress in Mammals? *Int. J. Mol. Sci.* **2024**, *25*, 1342. [CrossRef]
92. Gudkov, S.V.; Garmash, S.A.; Shtarkman, I.N.; Chernikov, A.V.; Karp, O.E.; Bruskov, V.I. Long-lived protein radicals induced by X-ray irradiation are the source of reactive oxygen species in aqueous medium. *Dokl. Biochem. Biophys.* **2010**, *430*, 1–4. [CrossRef]
93. Gudkov, S.V.; Shtarkman, I.N.; Chernikov, A.V.; Usacheva, A.M.; Bruskov, V.I. Guanosine and inosine (riboxin) eliminate the long-lived protein radicals induced X-ray radiation. *Dokl. Biochem. Biophys.* **2007**, *413*, 50–53. [CrossRef]
94. Gudkov, S.V.; Li, R.; Serov, D.A.; Burmistrov, D.E.; Baimler, I.V.; Baryshev, A.S.; Simakin, A.V.; Uvarov, O.V.; Astashev, M.E.; Nefedova, N.B.; et al. Fluoroplast Doped by Ag_2O Nanoparticles as New Repairing Non-Cytotoxic Antibacterial Coating for Meat Industry. *Int. J. Mol. Sci.* **2023**, *24*, 869. [CrossRef]
95. Serov, D.; Burmistrov, D.; Simakin, A.; Astashev, M.; Uvarov, O.; Tolordava, E.; Semenova, A.; Lisitsyn, A.; Gudkov, S. Composite Coating for the Food Industry Based on Fluoroplast and ZnO-NPs: Physical and Chemical Properties, Antibacterial and Antibiofilm Activity, Cytotoxicity. *Nanomaterials* **2022**, *12*, 4158. [CrossRef]
96. Serov, D.A.; Baimler, I.V.; Burmistrov, D.E.; Baryshev, A.S.; Yanykin, D.V.; Astashev, M.E.; Simakin, A.V.; Gudkov, S.V. The Development of New Nanocomposite Polytetrafluoroethylene/Fe_2O_3 NPs to Prevent Bacterial Contamination in Meat Industry. *Polymers* **2022**, *14*, 4880. [CrossRef]
97. Khruengsai, S.; Sripahco, T.; Rujanapun, N.; Charoensup, R.; Pripdeevech, P. Chemical composition and biological activity of Peucedanum dhana A. Ham essential oil. *Sci. Rep.* **2021**, *11*, 19079. [CrossRef]
98. Yong, S.-S.; Lee, J.-I.; Kang, D.-H. TiO_2-based photocatalyst Generated Reactive Oxygen Species cause cell membrane disruption of Staphylococcus aureus and Escherichia coli O157:H7. *Food Microbiol.* **2023**, *109*, 104119. [CrossRef]
99. Khater, M.S.; Kulkarni, G.R.; Khater, S.S.; Gholap, H.; Patil, R. Study to elucidate effect of titanium dioxide nanoparticles on bacterial membrane potential and membrane permeability. *Mater. Res. Express* **2020**, *7*, 035005. [CrossRef]
100. Rathore, C.; Yadav, V.K.; Gacem, A.; AbdelRahim, S.K.; Verma, R.K.; Chundawat, R.S.; Gnanamoorthy, G.; Yadav, K.K.; Choudhary, N.; Sahoo, D.K.; et al. Microbial synthesis of titanium dioxide nanoparticles and their importance in wastewater treatment and antimicrobial activities: A review. *Front. Microbiol.* **2023**, *14*, 1270245. [CrossRef]
101. Leung, Y.H.; Xu, X.; Ma, A.P.Y.; Liu, F.; Ng, A.M.C.; Shen, Z.; Gethings, L.A.; Guo, M.Y.; Djurišić, A.B.; Lee, P.K.H.; et al. Toxicity of ZnO and TiO_2 to Escherichia coli cells. *Sci. Rep.* **2016**, *6*, 35243. [CrossRef]
102. Muraro, P.C.L.; Wouters, R.D.; Chuy, G.P.; Vizzotto, B.S.; Viana, A.R.; Pavoski, G.; Espinosa, D.C.R.; Rech, V.C.; da Silva, W.L. Titanium dioxide nanoparticles: Green synthesis, characterization, and antimicrobial/photocatalytic activity. *Biomass Convers. Biorefinery* **2023**, *14*, 25279–25292. [CrossRef]

103. Younis, A.B.; Haddad, Y.; Kosaristanova, L.; Smerkova, K. Titanium dioxide nanoparticles: Recent progress in antimicrobial applications. *WIREs Nanomed. Nanobiotechnology* **2022**, *15*, e1860. [CrossRef]
104. Gudkov, S.V.; Sarimov, R.M.; Astashev, M.E.; Pishchalnikov, R.Y.; Yanykin, D.V.; Simakin, A.V.; Shkirin, A.V.; Serov, D.A.; Konchekov, E.M.; Gusein-zade, N.; et al. Modern physical methods and technologies in agriculture. *Physics-Uspekhi* **2024**, *67*, 194–210. [CrossRef]
105. Zore, A.; Abram, A.; Učakar, A.; Godina, I.; Rojko, F.; Štukelj, R.; Škapin, A.S.; Vidrih, R.; Dolic, O.; Veselinovic, V.; et al. Antibacterial Effect of Polymethyl Methacrylate Resin Base Containing TiO_2 Nanoparticles. *Coatings* **2022**, *12*, 1757. [CrossRef]
106. Bakr, A.M.; Darwish, A.; El Awady, M.E.; Hamed, A.A.; Azab, A.A.; Elzwawy, A. Physicochemical Evaluation of PMMA Doped TiO_2 Nanoparticles and Their Antimicrobial Features. *ECS J. Solid State Sci. Technol.* **2025**, *14*, 034001. [CrossRef]
107. Habib, S.; Rashid, F.; Tahir, H.; Liaqat, I.; Latif, A.A.; Naseem, S.; Khalid, A.; Haider, N.; Hani, U.; Dawoud, R.A.; et al. Antibacterial and Cytotoxic Effects of Biosynthesized Zinc Oxide and Titanium Dioxide Nanoparticles. *Microorganisms* **2023**, *11*, 1363. [CrossRef] [PubMed]
108. Tahir, H.; Rashid, F.; Ali, S.; Summer, M.; Abaidullah, R. Spectrophotometrically, Spectroscopically, Microscopically and Thermogravimetrically Optimized TiO_2 and ZnO Nanoparticles and their Bactericidal, Antioxidant and Cytotoxic Potential: A Novel Comparative Approach. *J. Fluoresc.* **2023**, *34*, 2019–2033. [CrossRef] [PubMed]
109. Qin, Q.; Li, J.; Wang, J. Antibacterial Activity Comparison of Three Metal Oxide Nanoparticles and their Dissolved Metal Ions. *Water Environ. Res.* **2017**, *89*, 378–383. [CrossRef] [PubMed]
110. Mendes, C.R.; Dilarri, G.; Forsan, C.F.; Sapata, V.d.M.R.; Lopes, P.R.M.; de Moraes, P.B.; Montagnolli, R.N.; Ferreira, H.; Bidoia, E.D. Antibacterial action and target mechanisms of zinc oxide nanoparticles against bacterial pathogens. *Sci. Rep.* **2022**, *12*, 2658. [CrossRef]
111. Sroila, W.; Kantarak, E.; Kumpika, T.; Bovonsombut, S.; Thongmanee, P.; Singjai, P.; Thongsuwan, W. Antibacterial activity absence UV irradiation of Ag, TiO_2 and ZnO NPs prepared by sparking method. *Mater. Today Proc.* **2019**, *17*, 1569–1574. [CrossRef]
112. Sánchez-Bodón, J.; Diaz-Galbarriatu, M.; Pérez-Álvarez, L.; Moreno-Benítez, I.; Vilas-Vilela, J.L. Strategies to Enhance Biomedical Device Performance and Safety: A Comprehensive Review. *Coatings* **2023**, *13*, 1981. [CrossRef]
113. *ISO 10993-1:2018*; Biological Evaluation of Medical Devices. ISO: Geneva, Switzerland, 2018.
114. Sevostyanov, M.A.; Kolmakov, A.G.; Sergiyenko, K.V.; Kaplan, M.A.; Baikin, A.S.; Gudkov, S.V. Mechanical, physical–chemical and biological properties of the new Ti–30Nb–13Ta–5Zr alloy. *J. Mater. Sci.* **2020**, *55*, 14516–14529. [CrossRef]
115. Chernikov, A.V.; Gudkov, S.V.; Shtarkman, I.N.; Bruskov, V.I. Oxygen effect in heat-induced DNA damage. *Biophysics* **2007**, *52*, 185–190. [CrossRef]
116. Ivanov, V.E.; Usacheva, A.M.; Chernikov, A.V.; Bruskov, V.I.; Gudkov, S.V. Formation of long-lived reactive species of blood serum proteins induced by low-intensity irradiation of helium-neon laser and their involvement in the generation of reactive oxygen species. *J. Photochem. Photobiol. B Biol.* **2017**, *176*, 36–43. [CrossRef]
117. Sevostyanov, M.A.; Baikin, A.S.; Sergienko, K.V.; Shatova, L.A.; Kirsankin, A.A.; Baymler, I.V.; Shkirin, A.V.; Gudkov, S.V. Biodegradable stent coatings on the basis of PLGA polymers of different molecular mass, sustaining a steady release of the thrombolityc enzyme streptokinase. *React. Funct. Polym.* **2020**, *150*, 104550. [CrossRef]

Disclaimer/Publisher's Note: The statements, opinions and data contained in all publications are solely those of the individual author(s) and contributor(s) and not of MDPI and/or the editor(s). MDPI and/or the editor(s) disclaim responsibility for any injury to people or property resulting from any ideas, methods, instructions or products referred to in the content.